LASER & PHOTONICS REVIEWS

www.lpr-journal.org

Novel Light Source Integration Approaches for Silicon Photonics

Zhechao Wang, Amin Abbasi, Utsav Dave, Andreas De Groote, Sulakshna Kumari, Bernadette Kunert, Clement Merckling, Marianna Pantouvaki, Yuting Shi, Bin Tian, Kasper Van Gasse, Jochem Verbist, Ruijun Wang, Weiqiang Xie, Jing Zhang, Yunpeng Zhu, Johan Bauwelinck, Xin Yin, Zeger Hens, Joris Van Campenhout, Bart Kuyken, Roel Baets, Geert Morthier, Dries Van Thourhout, and Gunther Roelkens*

Silicon does not emit light efficiently, therefore the integration of other light-emitting materials is highly demanded for silicon photonic integrated circuits. A number of integration approaches have been extensively explored in the past decade. Here, the most recent progress in this field is reviewed, covering the integration approaches of III-V-to-silicon bonding, transfer printing, epitaxial growth and the use of colloidal quantum dots. The basic approaches to create waveguide-coupled on-chip light sources for different application scenarios are discussed, both for silicon and silicon nitride based waveguides. A selection of recent representative device demonstrations is presented, including high speed DFB lasers, ultra-dense comb lasers, short (850nm) and long (2.3μm) wavelength lasers, wide-band LEDs, monolithic O-band lasers and micro-disk lasers operating in the visible. The challenges and opportunities of these approaches are discussed.

Z. Wang, A. Abbasi, U. Dave, A. De Groote, S. Kumari, Y. Shi, B. Tian, K. Van Gasse, J. Verbist, R. Wang, W. Xie, J. Zhang, Y. Zhu, B. Kuyken, R. Baets, G. Morthier, D. Van Thourhout, G. Roelkens
Photonics Research Group
Department of Information Technology (INTEC)
Ghent University - imec
Technologiepark-Zwijnaarde 15, B-9052 Gent, Belgium
E-mail: Zhechao.Wang@ugent.be

Z. Wang, A. Abbasi, U. Dave, A. De Groote, S. Kumari, Y. Shi, B. Tian, K. Van Gasse, R. Wang, W. Xie, J. Zhang, Y. Zhu, J. Bauwelinck, X. Yin, Z. Hens, B. Kuyken, R. Baets, G. Morthier, D. Van Thourhout, G. Roelkens
Center for Nano- and Biophotonics (NB-Photonics)
Ghent University
Technologiepark-Zwijnaarde 15, B-9052 Gent, Belgium

B. Kunert, C. Merckling, M. Pantouvaki, J. Van Campenhout
IMEC
Kapeldreef 75, 3001 Heverlee, Belgium

J. Bauwelinck, X. Yin
IDLab, Department of Information Technology
Ghent University - imec
Technologiepark-Zwijnaarde 15, B-9052 Gent, Belgium

Z. Hens
Department of Inorganic and Physical Chemistry
Ghent University
Krijgslaan 281 - building S3 (Campus Sterre), B-9000 Gent, Belgium

DOI: 10.1002/lpor.201700063

1. Introduction

A tremendous research effort has gone into the development of silicon photonics over the past decade. By leveraging the well-established complementary metal oxide semiconductor (CMOS) manufacturing infrastructure, silicon photonics allows for mass-producible, high-yield photonic chips. Relevant technologies have advanced such that most of the key components are nowadays available with superior performance, such as low-loss waveguides, multiplexing units, high-speed modulators and photodetectors. Thus, after years of R&D and investments by industrial giants and research centers, silicon photonics-based optical interconnect solutions are now finding their application in hyper-scale datacenters, a market that has traditionally been dominated by III-V-based solutions such as vertical cavity surface emitting lasers (VCSELs). On the other hand, despite that they are being processed on smaller wafers, with a lower process maturity, yield and therefore higher cost, compound semiconductor solutions are still dominating the discrete photonic devices market today. One of the key factors that holds back silicon photonics is that it is fundamentally very challenging to achieve efficient light generation, and subsequently realize lasing using silicon. Different from direct bandgap materials (such as GaAs and InP), the X valley of silicon's conduction band is not aligned with the maximum of its valence band. By the law of momentum conservation, to generate a photon by carrier recombination, a third particle (a phonon in this case) must be involved to carry away the excess momentum, which makes this process inefficient. For more details of the fundamentals and relevant research progress in silicon light emission, readers are referred to an earlier review article.[1]

Limited by the lack of efficient on-chip light sources, most of the demonstrated silicon photonic systems rely on external light sources. The use of off-chip lasers allows keeping their optimized performance in terms of efficiency, temperature control and long-term reliability. However, the output from off-chip lasers suffers extra loss when coupled into silicon photonic chips.[2]

The large physical footprint and the high cost of packaging also hinder the further scaling of the number of light sources that can be integrated on a single chip, which is particularly important when extending the transmission bandwidth using wavelength multiplexing. Therefore, a lot of research is geared towards integrating light sources on silicon photonic chips. In the past decade, several promising approaches have been extensively investigated, and improved light generation efficiency and even lasing have been demonstrated using Si nanocrystals,[3] rare earth doped glasses,[4] Germanium (Ge) and its alloys,[5,6] and Si-integrated III-Vs,[7,8] etc. An excellent review on these topics has recently been published elsewhere.[9] Considering that the above-mentioned research activities are all aligned with the aim of delivering on-chip light sources for optical interconnects, most of the demonstrations have been focusing on the following requirements: emission at communication wavelengths (1310 nm or 1550 nm); electrical pumping; operation at room or even elevated temperatures, low power consumption, and CMOS-compatible mass-production capability. On the other side, after being heavily investigated for over a decade, silicon photonics is going beyond a technology that is purely communication-oriented and has evolved into a versatile integration platform, which has a great potential to serve various application fields, including sensing,[10] spectroscopy,[11] signal processing,[12] quantum science,[13] microwave engineering,[14] imaging,[15] high performance computing,[16] etc. Depending on the nature of different application scenarios, some of the restrictions discussed above can be lifted, although new requirements may apply. In this work, we will review, non-exhaustively, novel light sources and integration approaches on silicon photonics that have been proposed and studied over the past few years. A summary of the recent progress will be made, and an assessment will be presented from the perspective of technological maturity, scalability, cost, and potential limitations. This paper is arranged as follows. Section 2 discusses the recent progress in wafer bonded III-V lasers on silicon. Besides newly developed high-speed lasers that benefit the traditional field of datacom and telecom, new laser configurations and the extension of the emission wavelength range hold great promise for sensing, spectroscopy, radio-over-fiber and microwave photonic applications. The use of III-V-on-silicon nonlinear waveguides for the spectral broadening of semiconductor mode-locked laser based frequency combs is described as well. Section 3 discusses a transfer printing integration approach, which is anticipated to replace bonding technology for III-V light source integration for relatively large volume applications. Basic principles will be covered, as well as a summary of recent demonstrations. Section 4 focuses on monolithically integrated III-V lasers, representing the ultimate solution for silicon-integrated light sources. A lot of progress has been made in the past few years, and we will focus on the newly demonstrated lasers based on localized epitaxial growth techniques. Section 5 discusses the potential application of colloidal quantum dots as a gain material for ultra-low power consumption and cost-effective light sources on silicon. In addition to a discussion of lasing in the visible wavelength range at room temperature, a new integration approach will be elaborated, which may lead to the ultimate co-integration of single photon sources with silicon photonic integrated circuits. In the final section, a comparison of all the topics covered will be presented, which is followed by a discussion of the perspective of this research field.

Zhechao Wang received his B. S. degree in Optical Engineering from the Zhejiang University, Hangzhou, China in 2005, and his Ph. D. degree in Applied Physics from the Royal Institute of Technology, Stockholm, Sweden in 2010. He joined Photonics Research Group, Ghent University, Belgium, as a post-doctoral researcher from 2011 to 2014. In 2015, he joined IMEC, Belgium as a researcher. He is currently a Photonics Scientist of Keysight Lab, California, United States of America. His research interests are primarily concerned with optoelectronic devices, heterogeneous integrated silicon light sources, and their applications in the fields of communication, instrumentation and imaging systems.

2. Heterogeneously Integrated III-V/Si Lasers

2.1. Introduction

Because of the direct bandgap and the high optical gain of III-V semiconductors, it is very appealing to integrate IIII-V lasers on silicon. Directly mounting pre-fabricated III-V lasers using flip-chip or pick-and-place technology is currently preferred by the industry.[2,17] It allows the pre-selection of known-good lasers, however the limited alignment tolerance and the high packaging cost make it unsustainable for further scaling. Therefore, wafer-bonding-based heterogeneous integration has been widely explored in the past decade and has proven to be the most successful approach up to now for dense III-V laser integration on silicon. Several bonding techniques, such as direct bonding and adhesive bonding, have been utilized to demonstrate various laser sources on silicon, including Fabry-Perot lasers,[8] distributed feedback (DFB) lasers,[18] micro-disk/ring lasers,[19,20] tunable lasers,[21] multi-wavelength lasers,[22] mode-locked lasers,[19] etc. Technical details of different bonding processes and a review of previous laser demonstrations can be found elsewhere.[23]

In the past few years, heterogeneously integrated III-V/Si lasers keep evolving at a rapid pace. By leveraging the low loss (< 1 dB/cm) of passive silicon waveguides, various laser configurations have been implemented for realizing narrow linewidth and low phase noise lasers,[24–26] widely tunable lasers,[24,27–29] and multi-wavelength lasers,[28,30,31] all of which are highly demanded for next generation high capacity coherent communication systems. As an example, **Figure 1**a shows a schematic plot of a widely tunable III-V/silicon hybrid laser formed by integrating a 4-cm long low-loss silicon external cavity with III-V amplifiers. Wavelength tuning is realized through the Vernier filter effect formed by the drop port response of two ring resonators with slightly different radii. The laser operates in the O-band and covers a

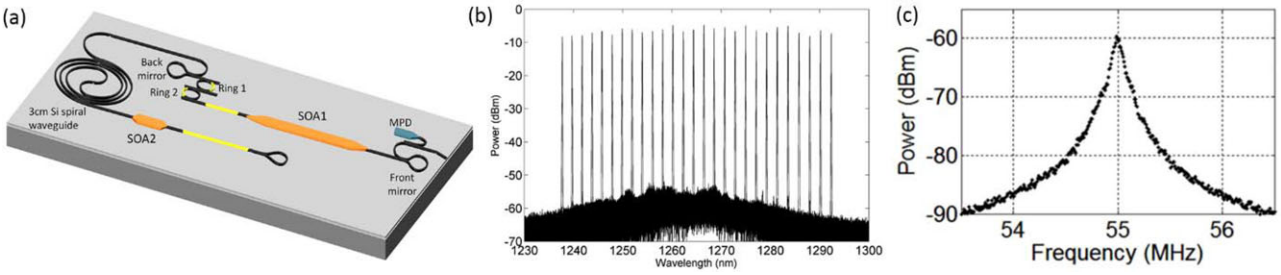

Figure 1. (a) A schematic view of a tunable laser design with integrated external cavity. Tuners are yellow and SOAs are dark orange. (b) Lasers are tunable over 54+ nm range with SMSR >45 dB (RBW–0.02 nm). (c) Measured spectrum showing a 50 kHz optical linewidth (3 MHz span, 30 kHz RBW). (Reproduced from[24])

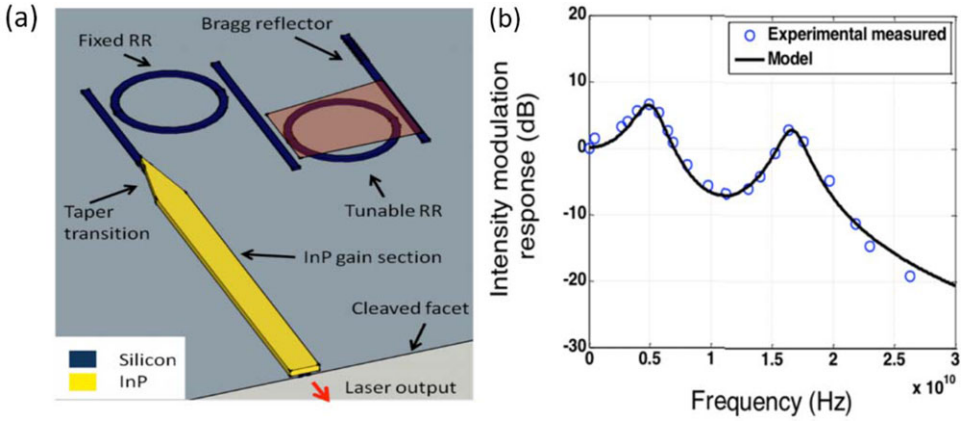

Figure 2. (a) Schematic structure of a heterogeneously integrated laser diode with feedback provided by a cleaved facet and a silicon double ring resonator structure. (b) Calculated and measured small signal modulation response. (Reproduced from[32])

54-nm wavelength tuning range as shown in Figure 1b. High side-mode suppression ratio exceeding 45 dB is achieved across the whole tuning range. Thanks to the controlled feedback from the external cavity, a narrow linewidth of 50 kHz (see Figure 1c) is achieved and the measured linewidth across the whole tuning range is below 100 kHz.

In recent years, there has been an increasing attention for the application of III-V/Si lasers as directly modulated optical transmitters for interconnects and passive optical networks. In the past, III-V-on-Si lasers operating at bit rates of 12.5 Gb/s and ~20 Gb/s have been demonstrated,[32,33] which is still significantly lower than the bit rates obtained with state-of-the-art monolithic InP DFB/DBR lasers[34] and long wavelength VCSELs.[35] The highest direct modulation speed for III-V-on-Si lasers had until recently been obtained for a laser with external cavity based on two cascaded ring resonators, as shown schematically in **Figure 2**. The high modulation bandwidth and bitrate are possible because of the so-called photon-photon resonance in the modulation response. This resonance occurs at a frequency equal to the inverse of the roundtrip time in the external cavity.[36] By leveraging the advances of III-V-on-Si lasers, fully integrated silicon photonic transceivers and interposers are also available nowadays.[37,38]

Besides traditional laser configurations, great progress has also been made in silicon-integrated micro-lasers and nanolasers. While optically pumped low threshold laser operation in nanolasers is widely demonstrated,[40] it is difficult to achieve efficient electrical injection due to the large nonradiative surface area, poor heat sinking, and the loss incurred from the electrodes.[41] Recently, highly efficient electrically pumped one-dimensional (1D) PhC nanolasers bonded on silicon waveguide circuit were demonstrated however.[39] A schematic of the hybrid nanolaser diode can be found in **Figure 3**. Great care is taken to design the electrodes properly to achieve a balance in injection efficiency and optical loss. Room temperature continue-wave (CW) lasing is achieved with a relatively low threshold of 100 μA and a wall-plug efficiency of more than 10%.

Following this discussion of the progress in heterogeneously integrated III-V/Si lasers, below we will review a selection of recent contributions to this field. Ultra-high-speed directly modulated lasers for optical interconnects are discussed in Section 2.2. Section 2.3 describes the recently demonstrated optical comb laser that holds promise for new applications such as dual-comb spectroscopy and microwave photonics. Section 2.4 discusses the possibility of further extending the optical comb span by integrating highly nonlinear III-V waveguides on silicon. Section 2.5 discusses lasers with an emission spectrum outside of the telecom band, suited for sensing applications.

2.2. Ultra-High Speed III-V/Si Lasers

Direct modulation at very high bit rates has recently been achieved for heterogeneously integrated InP/Si DFB lasers, of

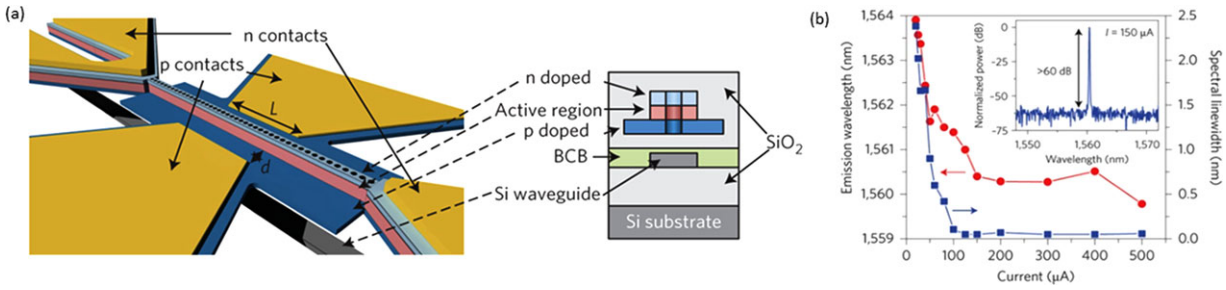

Figure 3. (a) Schematics of the hybrid nanolaser diode made of an InP-based 1D PhC nanocavity heterogeneously integrated with a SOI waveguide. (b) Wavelength and spectral linewidth of the light emitted by the nanolaser as a function of current. Inset: optical spectrum of the emitted light at I = 150 μA. (Reproduced from[39]).

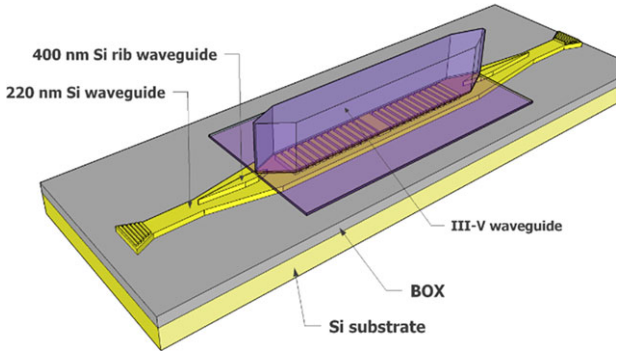

Figure 4. Schematic structure of a heterogeneously integrated InP/Si DFB laser diode. (Reproduced from[18])

which a schematic plot is shown in **Figure 4**. The small width of the InP ridge waveguides and the high refractive index contrast between InP and the surrounding divinylsiloxane-bis-benzocyclobutene (DVS-BCB) lead to high optical confinement in the active layer, which typically consists of 8 to 9 strained InGaAsP or InAlGaAs quantum wells.[42] Room temperature lasing with low threshold (below 20 mA for lasers of length 340 μm) and relatively high output power (5 mW) has been realized.[43] Furthermore, by making the bonding layer very thin (down to 10 nm), strong distributed reflections from the silicon grating characterized by a large coupling coefficient κ can be obtained. Since in strained layer multiple quantum wells the gain is approximately a logarithmic function of the carrier density, the combined large optical confinement factor and low mirror loss even for short cavity devices resulting from the large κ give a relatively high modal differential gain.

It is well known that a high modal differential gain leads to a high relaxation resonance frequency at high bias current, which is clearly shown in the presented small signal modulation characteristics measured at 100 mA in **Figure 5**a. The existence of a second resonance frequency around 30 GHz is caused by the 4% reflection from the output grating couplers, which form an external cavity to the laser. In addition to these two resonances, one can also distinguish a low-frequency contribution. It is mainly due to the modulation of the coupling tapers between Si and III-V, which act as semiconductor optical amplifier. This effect can be suppressed by modulating only the laser. Figures 5b and c show the large signal modulation and transmission results at 56 Gbit/s. Using lasers with a small signal modulation bandwidth of 34 GHz, NRZ-OOK modulation at 56 Gb/s[44] and error-free transmission (after forward error correction) of this signal over 2 km of nonzero-dispersion shifted fiber (NZ-DSF) has been achieved. Bit rates of 56 Gb/s and more have also been demonstrated using Discrete Multi-tone (DMT) modulation or electro-absorption modulation by using the laser tapers.[45]

2.3. Ultra-Dense Optical Comb Laser

An optical frequency comb is a source with a spectrum consisting of an array of discrete, equally spaced longitudinal modes that are all phase locked. Optical-frequency combs provide the link between the radio frequency domain and the optical domain, which enables a wide range of exciting applications.[11,46–48] Many mechanisms have been explored for comb generation, including mode-locked fiber lasers,[49] mode-locked titanium-sapphire lasers,[50] intensity modulation of a CW laser[51] and strong nonlinear interactions.[52] Most of the solutions are bulky and expensive. Therefore, a chip-scale, low-power-consumption comb source that can be electrically pumped is highly demanded.

Monolithically integrated III-V mode-locked lasers (MLLs), acting as compact multi-wavelength sources for telecom, covering a repetition rate of 10 GHz to 100 GHz have been heavily investigated over the past two decades.[53] A few attempts of utilizing a long high-quality cavity to improve mode-locking performance have been made,[54–56] although the improved performance is not satisfactory due to the high III-V waveguide loss. One may bypass this obstacle by utilizing a hybrid integrated laser configuration that uses low-loss silicon waveguides as an external cavity and high performance III-V heterostructure for making semiconductor optical amplifiers (SOAs) and saturable absorbers (SAs).[25,57]

Figure 6 shows the schematic of the III-V/Si ultra-dense comb laser.[58,59] The III-V is integrated on the silicon-on-insulator wafer (400 nm Si device layer thickness) using a 30-nm thick DVS-BCB bonding layer (not shown in the figure). A long and low loss (0.7 dB/cm) silicon spiral waveguide of 37.4 mm length forms the major part of the long laser cavity. Two semiconductor optical amplifiers (one of which acts as a spot-size converter for efficient light coupling between III-Vs and silicon) are implemented to provide optical gain. Two distributed Bragg reflectors (DBR) are defined in the silicon waveguide to form the two mirrors of the cavity. To achieve mode-locking, a 40-μm-long SA is defined by etching two 15-μm wide isolation slots in the III-V

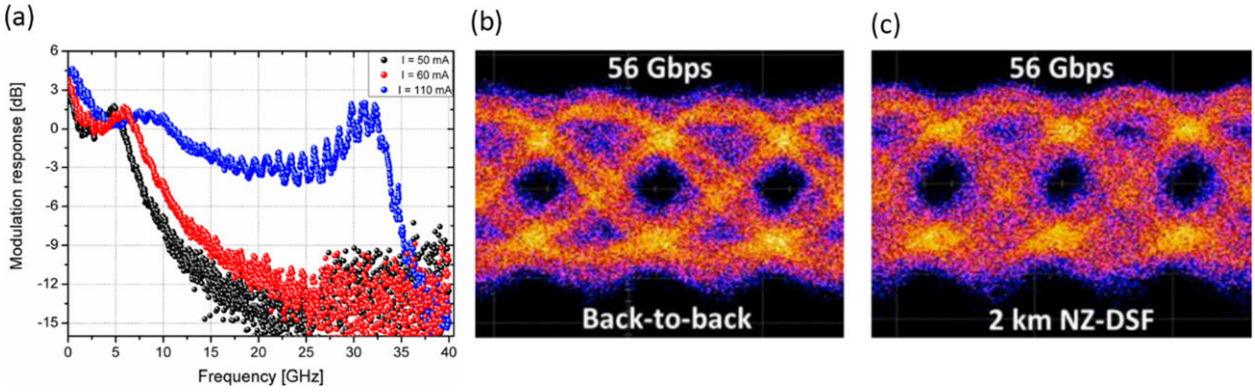

Figure 5. (a) Small signal modulation characteristics at 50 and 100 mA. (b) and (c) Eye diagrams for 43 Gb/s large signal modulation, measured back-to-back and after 2 km of NZ-DSF fiber (word length 2^7-1). (Reproduced from[44])

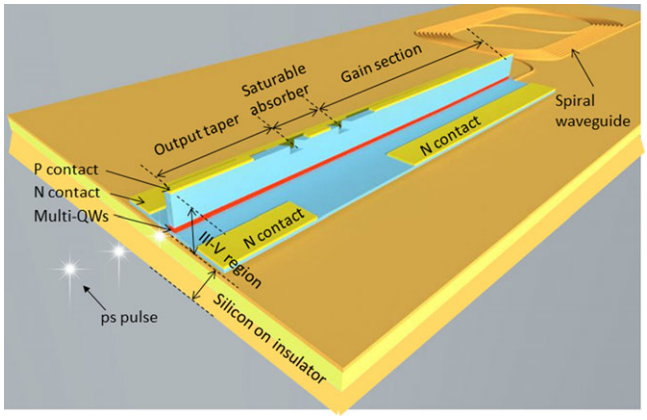

Figure 6. Schematic of the ultra-dense III-V/Si comb laser. (Reproduced from[58])

p-contact layer to electrically isolate it from the gain sections. Because both the amplifiers and the SA share the same InGaAsP-based multi-quantum well layer,[60] the fabrication process is easy to implement. Furthermore, by placing the SA above the DBR next to the output coupler, the MLL is working in anti-colliding pulse mode. It has been shown that anti-colliding operation enables higher output power, lower timing jitter, and better RF spectral purity.[61]

The III-V/Si MLL is passively locked at 1 GHz when the gain section is biased at 91 mA and the SA is reversely biased at -2.6 V. An overview of the measured high-resolution (5 MHz) optical spectrum of the laser output is presented in **Figure 7**a. The 10-dB optical bandwidth spans more than 15 nm. Considering that the line spacing of the longitudinal modes is only 1 GHz, this optical comb contains more than 1400 phase locked lines, which is the densest comb generated by an integrated MLL. The optical linewidth of the longitudinal modes is measured using a delayed self-heterodyne method (see Figure 7b). A narrow optical linewidth below 250 kHz is achieved, which surpasses other works[54–56] by at least one order of magnitude.

Figure 8a shows the measured RF spectrum of the pulse trains. The pure fundamental tone indicates high quality mode-locking with negligible residual amplitude modulation. From the insert, one can tell the 10-dB linewidth of the fundamental tone is below 900 Hz, which is much lower than in other integrated MLLs so far. In order to function as an optical comb generator, one needs to stabilize two degrees of freedom of the comb, which are the repetition rate (line spacing) and the offset frequency.[62] By supplying a RF reference signal to the SA, one may firmly stabilize the line spacing. Figure 8b presents the measured RF spectrum when the MLL is operating in a hybrid mode-locking mode. The linewidth of the fundamental tone is sub-Hz (not shown), which proves that the line spacing of the optical comb can be firmly stabilized. Regarding the offset frequency f_{ceo}, the widely used self-referencing method cannot be applied, because it is unlikely to generate an octave-spanning spectrum using integrated MLLs. However, one can resort to electronic feedback to stabilize f_{ceo}.[63] The optical comb can also be stabilized by locking the MLL to an external stable laser.[64]

2.4. III-V-on-Silicon Nonlinear Waveguides for Spectral Broadening

Broad optical combs that extend over an octave are highly demanded for metrology applications, which require strict stabilization of all degrees of freedom of the comb.[62] Although III-V-based comb lasers may never reach such wide frequency spans, one may exploit the strong third order nonlinear response, i.e. the Kerr material nonlinearity, of integrated waveguides for spectral broadening. One way of generating broadband combs is by pumping highly nonlinear high-Q resonators. When these resonators are pumped by a continuous wave signal a strong field builds up in these resonators. This enables to down and up convert photons in a four-wave mixing process and provides parametric gain near the pump wavelength. Although enormous progress has been made,[65–69] these combs typically need high threshold powers and can be difficult to bring in the coherent low noise comb state. Nevertheless, the nonlinear parametric gain has the enormous advantage of using virtual states and thus allowing for an almost limitless bandwidth. A particularly interesting demonstration, by M. Pu et al is comb generation in III-V AlGaAs-on-Si integrated micro-resonators.[69] The highly

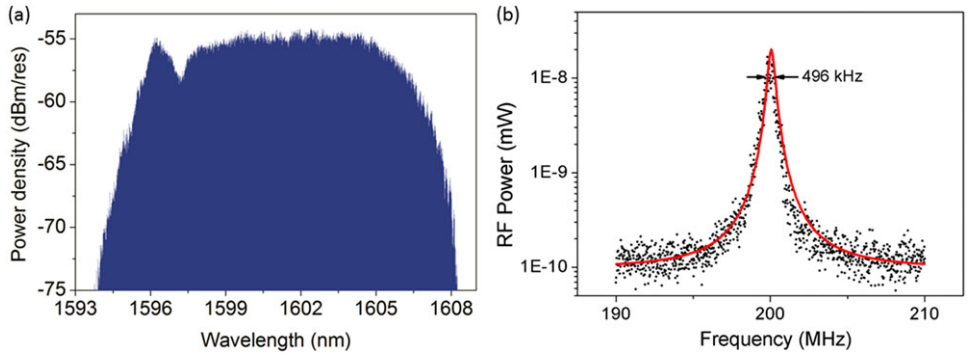

Figure 7. (a) Optical spectrum when the laser is passively locked at 1 GHz repetition rate. (b) Optical linewidth measured by using the delayed self-heterodyne method. The black dots are the measured data, and the red curve is the corresponding Lorentzian fitting. (Reproduced from[58]).

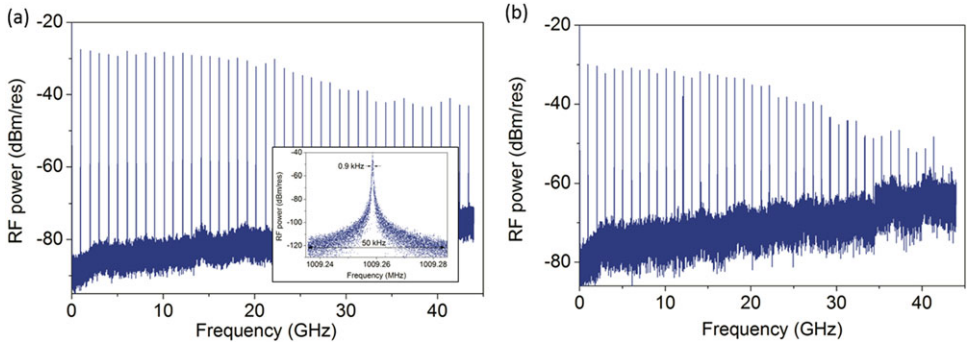

Figure 8. Measured RF spectra of the MLL output when it is (a) passively and (b) hybrid mode-locked. (Reproduced from[58]).

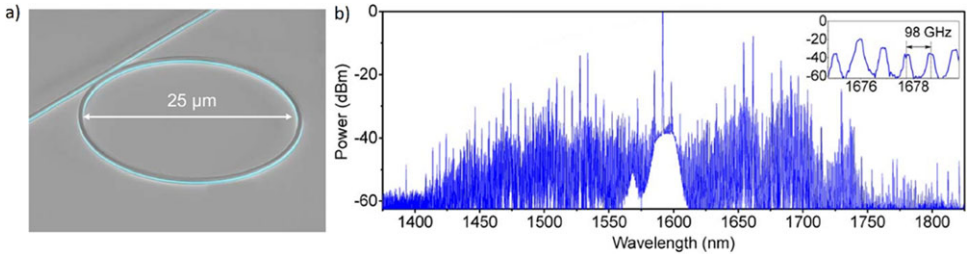

Figure 9. (a) A SEM picture of the integrated AlGaAs microresonator used in the comb generation experiment and (b) the generated output spectrum. (Reproduced from[69])

nonlinear response of the III-V waveguides allowed to lower the oscillation threshold down to a few mW. **Figure 9**a shows an SEM picture of the AlGaAs resonator, while in Figure 9b the broad bandwidth (>300 nm) bandwidth generated output comb spectrum can be seen.

One obstacle that makes a fully integrated comb generator challenging is that traditionally broadband combs are generated by pumping highly nonlinear waveguides with a seed comb. When additional bandwidth was needed, TiSapphire or fiber mode-locked laser combs underwent an extra broadening step in photonic crystal fibers. Building on this approach, we have recently shown that we can rely on heterogeneously integrated III-V InGaP nanowire waveguides bonded to oxidized silicon wafers[71] to broaden seed combs coherently.[70] Due to the very high nonlinear response of the waveguides and the absence of two-photon absorption in InGaP at telecom wavelengths this process can be very efficient. Although the interaction length in the waveguide was limited due to the relatively high losses of 12 dB/cm we succeeded in broadening 170 fs pulses with a peak power of merely 10 W up to an octave.[72] **Figure 10** shows the output spectrum of a 700-nm wide 250 nm high air clad InGaP waveguide of 2 mm when it is pumped by a pulse train increasing in power. It was confirmed that the comb like structure of the input source was preserved in the experiment. Lately, with the help of accurate theoretical models, the process of coherent comb generation is well understood,[73] which benefits various application fields.[74,75] The next step would be to integrate these spectral broadening devices with the III-V-on-silicon mode-locked lasers discussed above. When the losses of the waveguides could be reduced, as has been demonstrated in an AlGaAs-on-insulator platform,

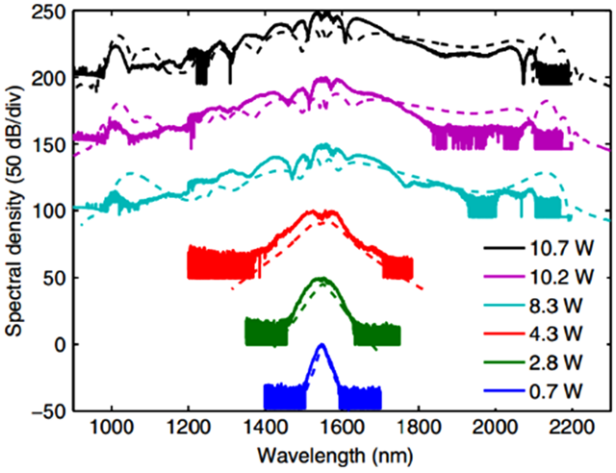

Figure 10. The output spectrum of the 2 mm InGaP wire waveguide when pumped by 170 fs pump pulses. It was confirmed that the process does not destroy the coherence of the input pulses. (Reproduced from[70])

this would allow to reduce the threshold for comb generation further and allow for a fully integrated octave spanning electrically pumped comb source. Again, this comb source would take the full advantage of the flexibility of the hybrid platform: it allows to combine low-loss silicon waveguides for the laser cavity, high-performance III-V gain material and high-performance nonlinear waveguides.

2.5. Laser Emission Beyond 1550/1310 nm

2.5.1. Silicon Integrated 2.x μm Laser for CO Sensing

Silicon photonics is also of interest for optical sensing in the 2–3 μm wavelength range as many important gases (e.g., CO_2, CH_4 and CO) have strong absorption lines in this wavelength range. Compact spectroscopic gas sensors can be realized by heterogeneously integrating III-V laser sources and detectors on passive silicon PICs. The emission wavelength of heterogeneous III-V/silicon laser sources has been extended to around 2 μm based on highly strained InP-based type-I heterostructures.[76] But the emission wavelength of this material system is limited to around 2.3 μm. Above 2.3 μm wavelength, GaSb-based heterostructures can be used to realize lasers with high performance. However, the heterogeneous integration of GaSb-based material is much less established than is the case for InP-based material. Recently, we demonstrated the heterogeneous integration of III-V/silicon laser sources emitting beyond 2.3 μm, by integrating InP-based type-II heterostructures on silicon PICs.[77–79]

A typical emission spectrum of a heterogeneous DFB laser designed for CO gas sensing is shown in **Figure 11**a. A SMSR of 40 dB is obtained. In a CW regime, the 2.32 μm DFB laser works close to room temperature (>15 °C), has a maximum output power of 1.3 mW and a threshold current density of 1.8 kA/cm^2 at 5 °C. Tuning of the emission wavelength by means of varying the injection current is also demonstrated, which enables tunable diode laser absorption spectroscopy (TDLAS). The measured current-tuning rate is 0.01 nm/mA. Over the whole bias current range, single mode lasing is achieved for a heat-sink temperature variation from 5°C to 15°C. Direct absorption spectroscopy of CO is carried out by tuning the laser emission wavelength by changing the bias current. The TDLAS spectrum of CO is obtained as shown in Figure 11b. The measurement results fit well to the high-resolution transmission molecular absorption database (HITRAN) data. As type-II lasers on InP substrate with emission wavelength up to 2.7 μm were demonstrated recently,[80] the operating wavelength of the heterogeneously integrated III-V/silicon PICs can be extended further to cover more gas absorption lines in the 2–3 μm wavelength window.

2.5.2. 850 nm Silicon-Integrated Vertical-Cavity Surface-Emitting Laser (VCSEL)

Integration of short-wavelength lasers on a silicon nitride waveguide platform on Si can enable fully integrated photonic circuits for applications in life sciences and short-reach optical interconnects. There have been reports on GaAs-based vertical-cavity surface-emitting lasers (VCSEL) with power conversion efficiencies exceeding 60%, modulation bandwidths up to 30 GHz,[81] and data rates exceeding 70 Gb/s.[82] Therefore, it is an attractive source for integration on a silicon nitride waveguide platform for applications requiring wavelengths in the range ~650 –1100 nm.

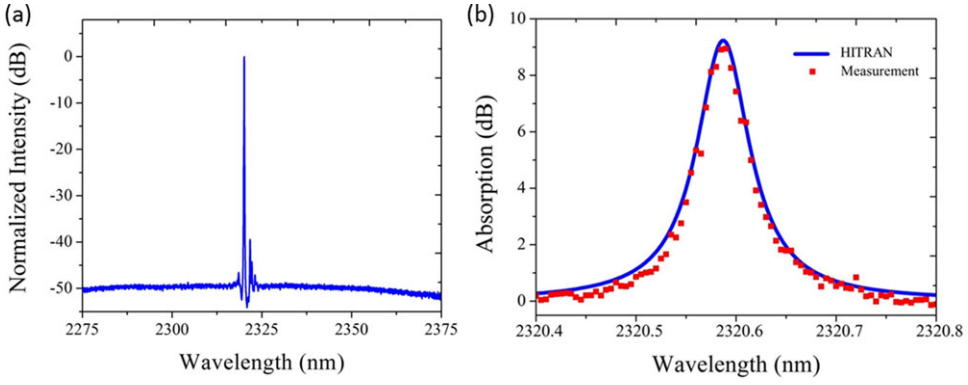

Figure 11. (a) Emission spectrum of the InP/Si type-II DFB laser; (b) TDLAS spectrum of CO and the corresponding high-resolution transmission molecular absorption database (HITRAN) spectrum. (Reproduced from[78])

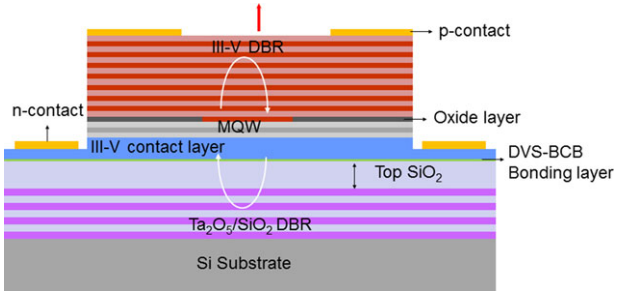

Figure 12. Schematic of the surface emitting HC-VCSEL. (Reproduced from[89]).

VCSELs have been integrated with Si waveguide by flip chipping them onto a perfectly vertical grating coupler,[83] or onto an angled grating coupler.[84,85] The monolithic integration of VCSELs and waveguides has also been demonstrated where the VCSEL is integrated with planar Si waveguide using Si high contrast grating (HCG)[86,87] and to a III-V waveguide by an integrated Bragg diffraction grating placed inside the top p-DBR.[88]

Recently, we demonstrated silicon-integrated GaAs-based hybrid-cavity vertical cavity surface emitting lasers (HC-VCSELs) operating at 850 nm.[89–92] The HC-VCSEL, schematically shown in **Figure 12**,[89] consists of a top III-V "half-VCSEL" containing 23 pairs of p-doped $Al_{0.90}Ga_{0.10}As/Al_{0.12}Ga_{0.88}As$ DBR, a 30 nm thick $Al_{0.98}Ga_{0.02}As$ layer for the formation of an oxide aperture, an active region with 5 $In_{0.10}Ga_{0.90}As/Al_{0.37}Ga_{0.63}As$ multi-quantum wells (QWs), and an n-doped $Al_{0.12}Ga_{0.88}As$ intracavity contact layer. The bottom mirror is formed by a 20-pair SiO_2/Ta_2O_5 dielectric DBR on a Si substrate. The HC-VCSEL is constructed by attaching the top III-V "half-VCSEL" to the bottom dielectric distributed Bragg reflector on a Si substrate using ultra-thin DVS-BCB adhesive bonding.

These HC-VCSELs had an output power of 1.6 mW at 845 nm[89] and were capable of 20 Gb/s error-free data transmission under direct current modulation.[90] The bonding interface is found to be of high importance for the optimization of the laser performance.[91] By choosing the thickness of the bonding interface one can either achieve minimum threshold current, maximum output power and maximum bandwidth at a specific ambient temperature or a temperature-stable threshold current and bandwidth.

A comparison of four HC-VCSELs denoted A–D, with bonding interface thicknesses of 35, 65, 125, and 180 nm resulting in resonance wavelengths of 843, 853, 861, and 867 nm with gain-to-resonance detuning of approximately +9, −1, −9, and −15 nm, respectively were studied. The output power and voltage versus current measured at ambient temperatures ranging from 15 to 100 °C, in steps of 5 °C, are shown in **Figure 13**. While the threshold current of HC-VCSEL D is higher than that of HC-VCSEL B at 25°C, it is lower at high temperatures and shows a weaker dependence on temperature. This is due to the fact that the gain-resonance detuning of HC-VCSEL D at room temperature leads to an on-resonance behavior at high temperature, thereby resulting in a lower threshold current at high temperature compared to HC-VCSEL B, which is detuned at high temperature. Among the 4 different HC-VCSELs A-D, HC-VCSEL B and C produced the highest output power (2.3 mW) at 25 °C, whereas at higher temperature HC-VCSEL D showed improved performance due to gain peak alignment with the resonance wavelength at higher internal temperature. The performance of HC-VCSEL A was limited to the maximum operating temperature 70 °C due the rapid increase of threshold current with temperature, due to the already positive detuning at room temperature.

Figure 14 shows the modulation response for HC-VCSELs A–D at 25°C and 85°C, compensated for the frequency response of the probe and the photodetector. The bonding interface thickness also had an impact on the HC-VCSEL dynamics. HC VCSEL B-D had the most damped response at the highest current, due to differential gain being lower on the long-wavelength side of the gain peak. At 25°C HC-VCSEL B had the highest 3 dB modulation bandwidth (10.0 GHz) whereas at 85°C the HC-VCSEL D had the highest bandwidth (6.4 GHz). HC-VCSEL D also showed the smallest dependence of modulation bandwidth on temperature.

The next phase of this work is to integrate the above-discussed VCSELs with silicon nitride waveguides and relevant photonic devices, which may pave the way of realizing fully-integrated solutions for life science and short-reach optical interconnects applications.

3. Transfer Printing

3.1. Introduction

As described above, classical heterogeneous integration approaches rely on die-to-wafer or wafer-to-wafer bonding for the integration of III-V material. In many cases, however, such an approach is not efficient in terms of usage of III-V material. In most optical chips, the area taken by the III-V opto-electronic components is only a fraction of the circuit area. Moreover, integrating

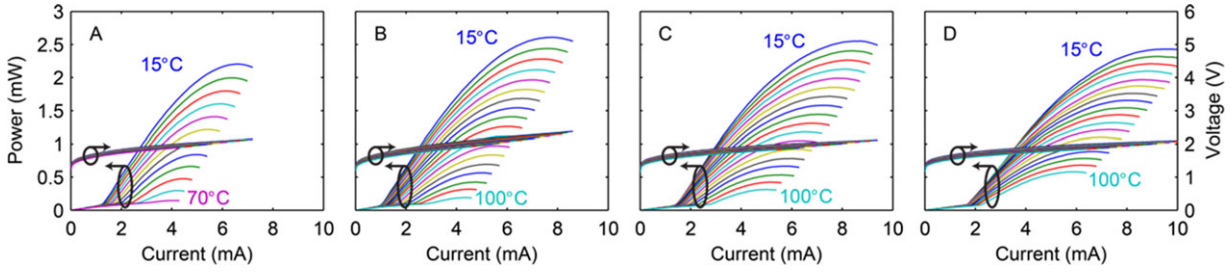

Figure 13. Output power and voltage versus current for HC-VCSELs A–D measured at ambient temperatures ranging from 15 to 100°C in steps of 5°C. (Reproduced from[91])

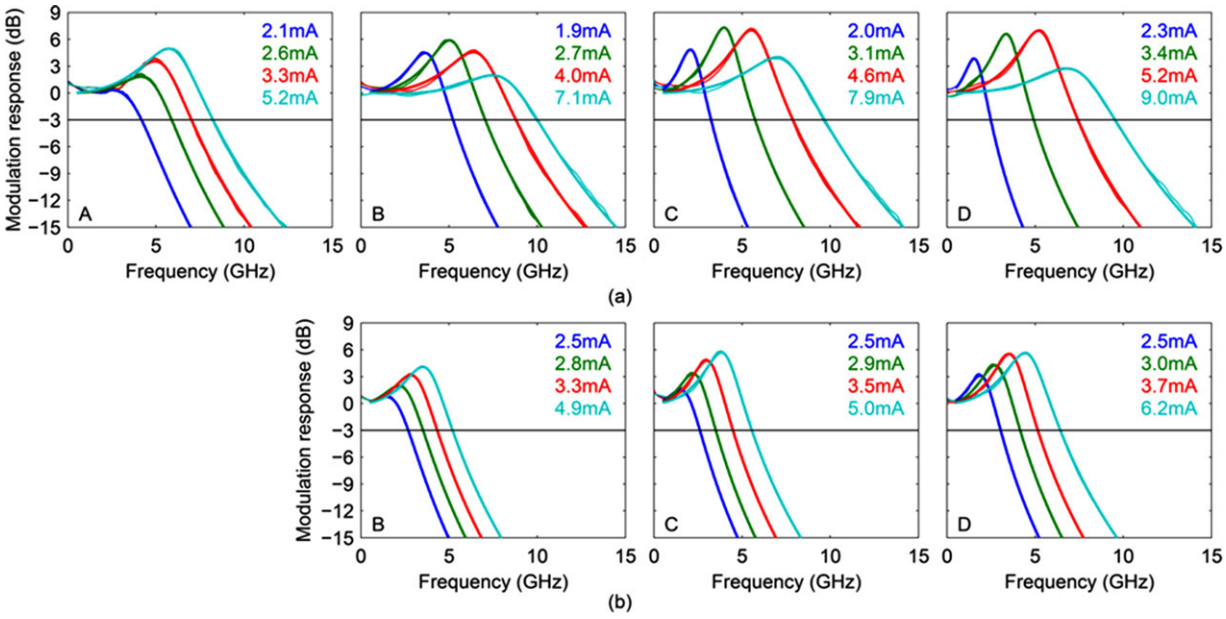

Figure 14. Small-signal modulation response at 25 °C (a) and 85 °C (b) for HC-VCSELs A–D at indicated bias currents. The maximum 3 dB modulation bandwidth is reached at the highest bias currents indicated. (Reproduced from[91])

different III-V layer stacks on a single chip leads to strong limitations in mask design because of the minimum sizes that are needed for the bonded dies. In 2004, Menard et al[93] proposed a novel technique, transfer printing, where micron-scale thin-film components can be transferred from a source substrate to a target substrate. This technique can be an enabling technology for the cost-effective integration of III-V semiconductor materials or devices on Si PICs, as it only provides III-V where it is needed, while maintaining high throughput and scalability. In the paragraphs below we will discuss the working principle of transfer printing and the benefits it brings. Next, we will discuss the demonstration of transfer-printed components on a silicon photonic circuit, after which the remaining challenges are listed.

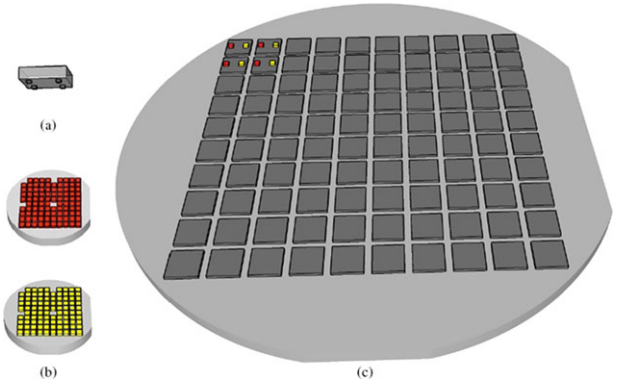

Figure 15. Illustration of area magnification in transfer printing of III-V coupons from the III-V source substrate to the SOI target substrate. The coupons of the first source wafer are indicated in red, the second one in yellow. (a) Patterned stamp (b) Two source substrates with patterned coupons, (c) SOI target substrate with four printed coupons from each source in the top left. (Reproduced from[95])

3.2. Working Principle

In transfer printing, a thin film material stack or device (hereafter referred to as a coupon) is transferred from a source substrate to a target substrate by use of a soft elastomeric PDMS stamp. As described elsewhere,[94] the adhesion to the elastomeric stamp depends on the velocity of the stamp. The coupon can be picked up from the native substrate by moving up the stamp rapidly (thus exerting a force greater than the adhesion to the native substrate), and printed to a Si PIC by releasing the stamp slowly. While showing similarities with a pick-and-place technique, the main advantage in transfer printing is that coupons can be transferred in a massively parallel way. Using a patterned stamp, which only contacts the substrates in selected positions, large arrays of coupons are picked and printed at the same time. This is shown in **Figure 15**, where all 4 red/yellow coupons were transferred in parallel (the array can consist of more than 4 coupons of course). The figure also illustrates so-called area magnification, where a small III-V wafer can populate multiple large Si wafers in a step and repeat manner. Integrating multiple III-V stacks can be done in a straight-forward manner by using multiple source wafers.

To be able to overcome the adhesion of the coupon to the substrate with the PDMS stamp, the coupon should be released from the III-V growth substrate. Therefore, the transfer printing technology differs from pick-and-place in the sense that the coupons are very thin, free-standing and substrate-free, which may pose some challenges as will be discussed later. During the release process, the entire coupon is undercut and is only supported by small tethers from the side, as shown in **Figure 16**. The coupons are patterned in two steps, after which they are encapsulated in photoresist and the tethers are formed. In the InP material system either an InGaAs or InAlAs release layer is used. The

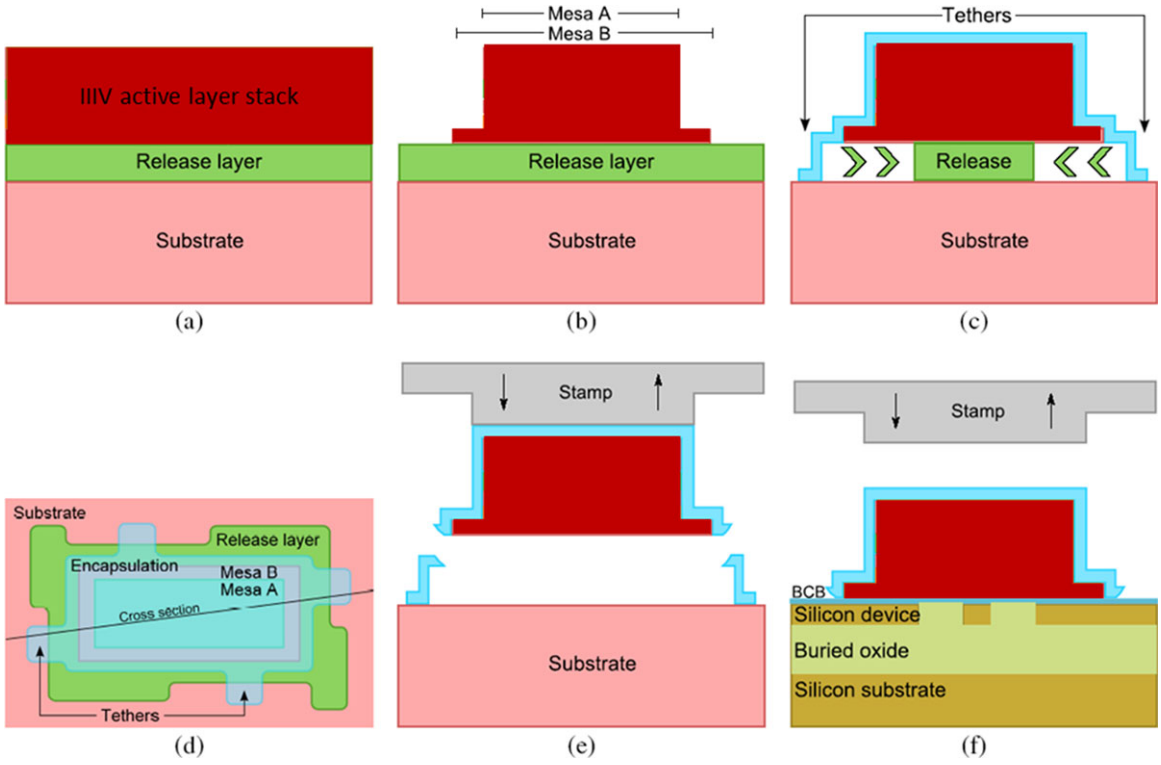

Figure 16. Release process for transfer printing. (a) InP starting layer stack, (b) coupon patterning, (c) Tether definition and release etch, (d) Top view, (e) Pick-up of the coupon from the source substrate, (f) Printing of the III-V coupon to the SOI target substrate

release layer is etched horizontally, undercutting the entire structure. The release etchant requires a selectivity of at least 1000, as several microns of release layer should be removed while only nanometers of the InP barrier layer can be etched. This has been optimized in,[95] where a cold, aqueous $FeCl_3$ etchant was identified to be most suited. Once released, the coupon is picked up by retracting the PDMS stamp rapidly, breaking the tethers. Printing is done slowly, letting the adhesion to the BCB-coated SOI circuit overcome the adhesion to the stamp.

3.3. Demonstrations

Several devices were successfully fabricated using this approach. J. Justice et al. presented a wafer-scale strategy for the integration of high-performance GaAs lasers on non-native substrates.[96] **Figure 17**a shows the schematic overview of the processing flow: a large number of coupons are transferred to a silicon substrate using a single transfer stamp and laser cavities are then defined using wafer-scale process techniques. Electrically pumped low threshold lasing at room and elevated temperatures was successfully achieved in the 800 nm wavelength range (see Figure 17b). At almost the same time, H. Yang et al. demonstrated an ultrathin DBR-free membrane reflector VCSEL on silicon, based on transfer-printing InGaAsP quantum well cavities and two sandwiching bottom and top silicon membrane reflectors.[97] A schematic of the MR-VCSEL and some SEM images of the fabricated devices can be found in **Figure 18**. By employing double silicon membrane reflectors, the VCSEL is very thin. Optically pumped room temperature lasing in the wavelength range of 1500 nm has been achieved (see Figure 18b). Besides the work mentioned above, light emitting diodes (LED) have also been integrated on mechanically-flexible substrates using similar technologies.[98]

The examples above integrate III-V with silicon, but do not couple to a silicon PIC. More recently coupling structures from the III-V to the Si PIC have also been designed and demonstrated.[95] Two approaches can be followed: one can transfer print the material and then pattern the device on the silicon target wafer, alternatively the device can be pre-fabricated on the InP wafer and then transfer printed with high alignment accuracy (+- 1.5μm 3σ). Below we discuss an example of both approaches, which serve as a stepping stone to more complex heterogeneously integrated circuits. A waveguide-coupled high-index-contrast light emitting diode (LED) can be used as broadband light source for sensing applications, thereby aiming at an efficient but simple and tolerant device. In,[95] InP high contrast membranes were transfer printed from an InP source wafer to an SOI target. Subsequently, optically pumped LEDs were fabricated in the transferred material. **Figure 19** shows the device design and operating principle as well as the measured spectrum when pumping the membrane with a 1310 nm pump laser. The measurements indicate that the power-efficiency is of the same order of magnitude as previously reported by traditional die-to-wafer heterogeneous integration. The 3-dB bandwidth of 130 nm is large and compares well to previously reported results. This confirms the bond when transfer printing is of the same quality as for traditional die-to-wafer or wafer-to-wafer methods.

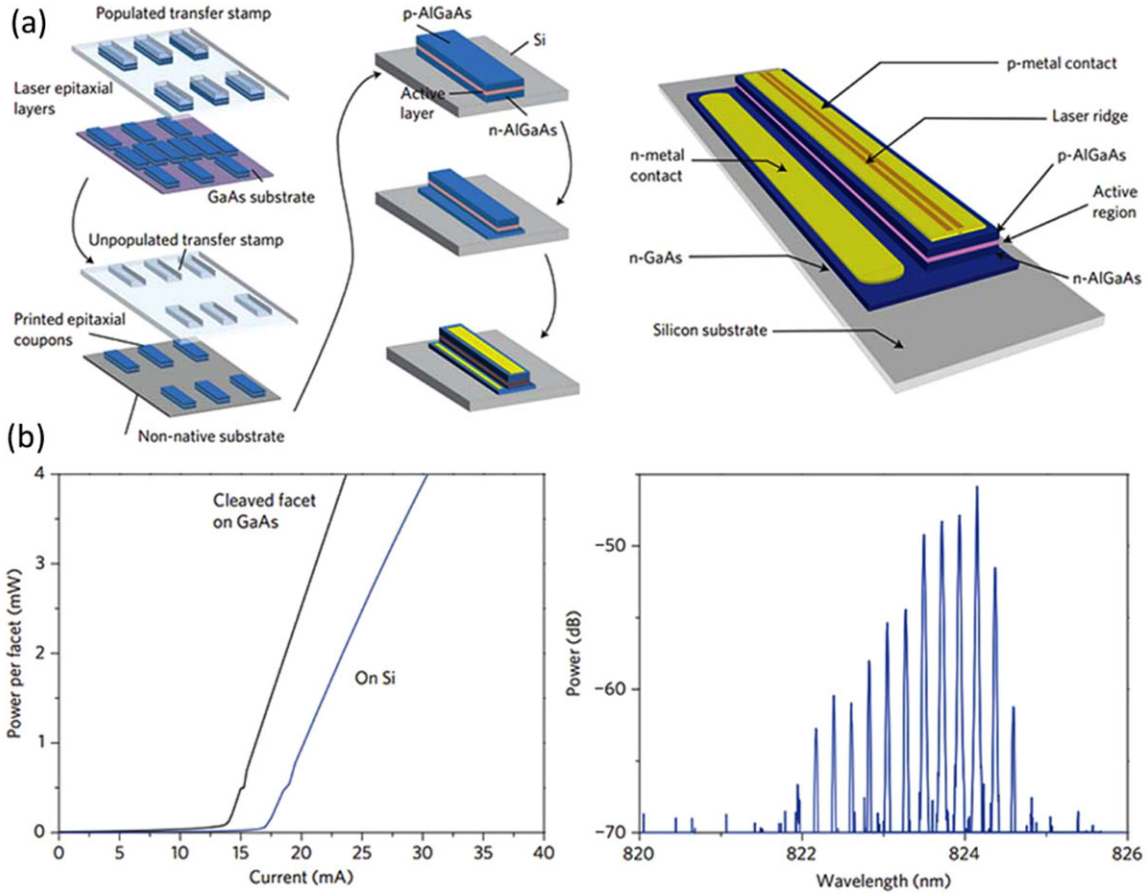

Figure 17. (a) Schematic overview of the integration process of group III-V lasers on silicon using transfer printing of epitaxial layers, with images of fabricated devices. (b) Characteristics of lasers fabricated on silicon. (Reproduced from[96])

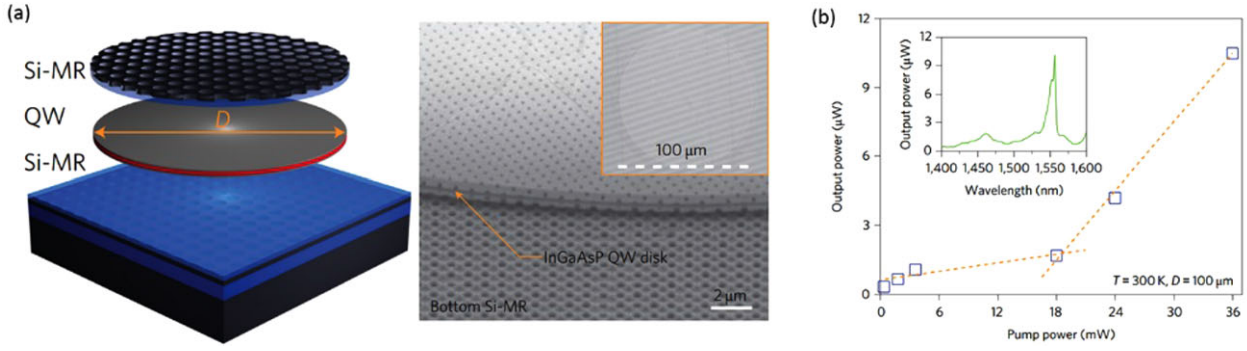

Figure 18. (a) Schematic plot of the silicon-integrated membrane reflector VCSEL (MR-VCSEL) and its multi-layer printing process, with images of fabricated devices. (b) Light in-light out (LL) curve and optical spectrum of the MR-VCSEL working at room temperature. (Reproduced from[97]).

A 4-channel transceiver for point-to-point Fiber-To-The-Home (FTTH) optical networks operating at 10 Gb/s was demonstrated by transfer printing pre-fabricated O-band III-V photodetectors (PDs) on top of silicon photonic grating couplers.[99,100] **Figure 20**a shows the pre-fabricated PDs on the InP substrate after the release etch. Note the high density of devices on the source wafer. Thanks to the pattern recognition function of the transfer printing system, the PDs were automatically aligned onto the grating couplers with good alignment accuracy. After the transfer printing a bond pad array was realized and connected to the predefined P and N metal of the photodiodes, as shown in Figure 20b. The PD is transparent for C-band signals but responds to O-band signals by designing the cut-off wavelength of the absorbing material to be 1.37 μm. The measurement result revealed a uniform responsivity of 0.4-0.5 A/W for these PDs while for C-band signals the responsivity was 0.025-0.03 mA/W, resulting in more than 40 dB suppression. The 30 by 40 μm large PDs have a 3 dB bandwidth of 11 GHz at -3 V bias. Figure 20c shows an

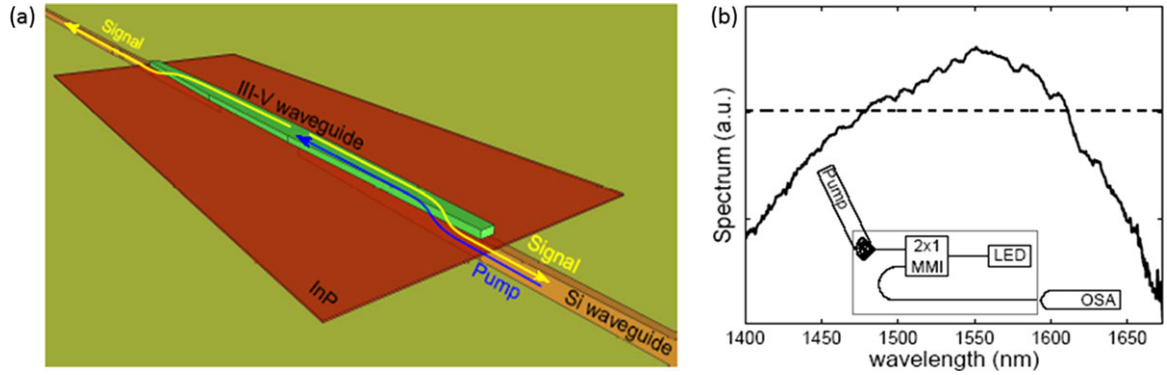

Figure 19. A transfer-printed, high-index-contrast LED. (a) Device design illustration, (b) Measurement results. (Reproduced from[95])

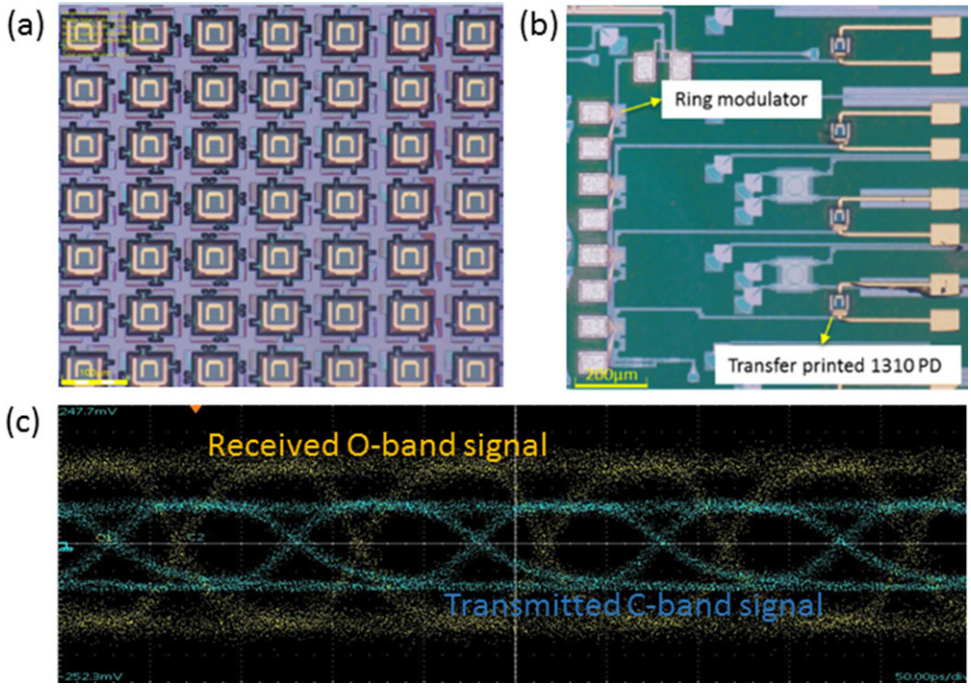

Figure 20. (a) Pre-defined PD array with contact metal on the III-V source wafer, (b) Microscope image of the 4-channel III-V on Si FTTH transceiver with printed PDs after final metallization, (c) Overlaid 10 Gbit/s eye diagrams of the received upstream (O-band) data signal and transmitted downstream (C-band) data signal. (Reproduced from[100])

overlaid eye diagram of both upstream (O-band) and downstream (C-band) signals at 10 Gb/s.

3.4. Challenges

In the last years we have been steadily moving towards transfer printed optical devices coupling to Si PICs, starting with III-V devices printed on a silicon substrate[96–98,101] and now moving on to simple devices coupling to SOI.[95,100] For the transfer-printing-based integration of light sources on Si PICs, there are still a few challenges ahead though.

So far, the transfer printed coupons coupling to the Si PIC have been small (below 100 μm a side). While a width of a few 10s of microns is sufficient for e.g. lasers, a length of several 100 microns will be required. As mentioned above, the coupon is released from the source substrate prior to pick-up. Due to the increased length, stress in the layer stack might bend or twist the free-hanging coupon, which in turn would decrease the bonding quality. Previously this was solved by using thick adhesive layers, but this prevents coupling to the underlying silicon waveguides. Especially when transferring sheet material and fabricating the device on the silicon chip, the bond needs to be of excellent quality as many aggressive etchants will be used in the post-bond process.

For the transfer printing of fabricated devices, alignment becomes of major importance. Several coupling structures tolerant to misalignment (1.5 μm 3σ) have been designed,[102] but so far no such devices have been realized. Giving the current speed of development of transfer printing for optics, we believe these challenges will be overcome in the time to come.

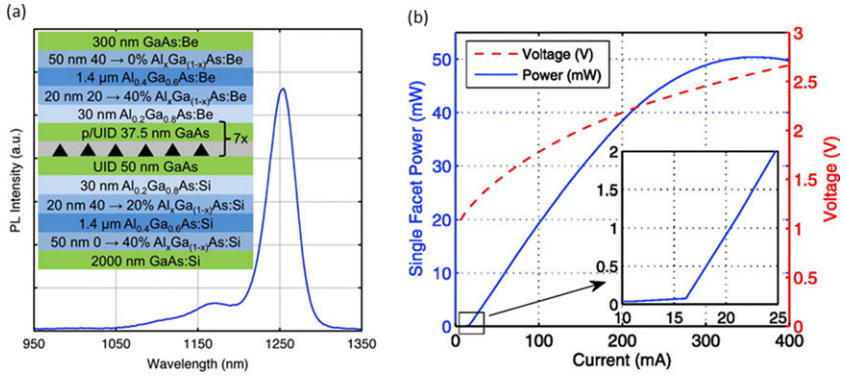

Figure 21. (a) Room temperature photoluminescence spectrum of the InAs quantum dots grown on Ge-on-Si substrates (inset: layer structure of the QD laser). (b) LIV plot of a 937 × 4 μm^2 laser. (Reproduced from[108])

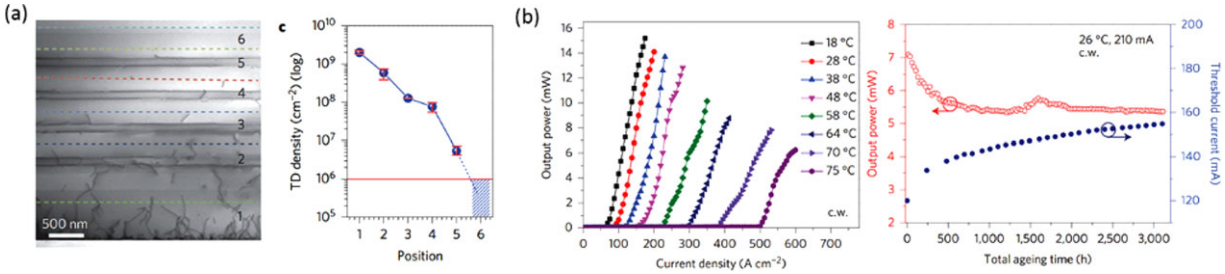

Figure 22. (a) Structural and material characterization of the QD heterostructure directly grown on silicon. (b) Characterization results of a room-temperature operating InAs/GaAs QD laser grown on a silicon substrate. (Reproduced from[109])

4. Monolithic Integrated III-V/Si Lasers

4.1. Introduction and Recent Progress

Wafer bonding provides the freedom of combining very different materials on a single wafer and transfer printing takes a step forward reducing the cost of this process and rendering it suitable for medium-to-large-volume applications. However, being able to epitaxially grow and thereby monolithically integrate III-V lasers directly on silicon remains the ultimate goal. By the monolithic integration one may fully enjoy the economics of scale promised by silicon photonics. For applications such as on-chip interconnect, the required number of optical channels may exceed 1000 to reach a total bandwidth of around 10 Tbit/s by assuming 10 Gbit/s per channel.[103] Such large number of lasers may only be met economically by a monolithic integration approach. On the other hand, the challenges are enormous. The large mismatch in lattice constant (8% for InP/Si and 4% for GaAs/Si) makes it very difficult to coherently grow III-Vs on silicon. The misfit and thereafter threading dislocations generated during growth are detrimental for laser operation and can substantially degrade the laser performance over time. Making things even worse is the polarity mismatch of III-V semiconductors and silicon. When growing polar III-Vs on nonpolar silicon, so-called anti-phase boundaries (APBs) appear when the islands of III-Vs grown during the initial steps of the process merge with each other. Therefore, although being investigated over several decades, not much progress has been reported until this topic regained momentum a few years ago, driven by the big investments of the electronics industry in developing high-mobility channel materials for next generation transistors. Consequently, considerable progress has been made in the last few years.[104–107] The community currently is embracing the insertion of quantum dot III-V active regions for both dislocation filtering and as advanced gain material. It has been demonstrated that a few well-optimized quantum dot layers can function as efficient defect filters that bend threading dislocations downwards,[108,109] allowing to make the buffer layer between III-Vs and silicon considerably thinner than before.[110] **Figure 21** shows that by growing multiple strained-layer superlattices (SLSs) as dislocation filter layers (DFLs), the threading dislocation density has been substantially reduced. Furthermore, by using quantum dots as the gain material, the laser is more immune to dislocations because a line defect only affects a few quantum dots while the rest of the gain layer remains of high quality. Independently, researchers from UCSB and UCL demonstrated room temperature lasing with high output power and reliability[108,109] (see Figure 21 and **Figure 22**). It is worth to mention that the long term mean time to failure (MTTF) in[81] is estimated to be over 100,158 h (see Figure 22b), which shows that QD III-V-on-Si lasers are very appealing for practical applications.

One obstacle that the QDs-based approach needs to overcome is the anti-phase boundaries, which cannot be removed by filtering. The widely-used offcut silicon substrates are not used by the CMOS industry. However, the recent demonstration of an InAs QD micro-disk laser grown on (001) Si provides encouraging progress.[105] Besides, the group at UCL made a significant progress by demonstrating monolithic III-V lasers on APB-free GaAs-on-Si substrate,[111] showing it is indeed feasible to work with standard silicon wafers.

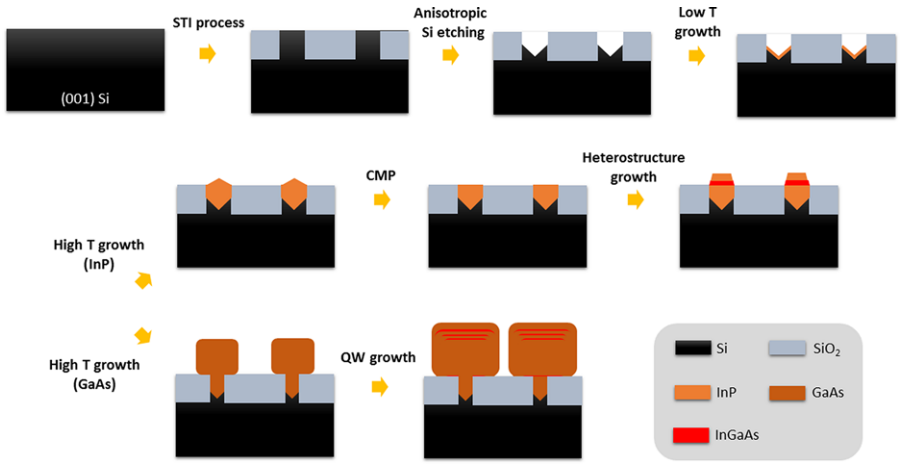

Figure 23. Selective growth of InP/GaAs on pre-patterned (001) Si substrates.

Beyond InP and GaAs, some other, relatively new material systems are also investigated. For example, GaP-related materials as GaNAsP can be engineered to have very small lattice mismatch such that they can be grown on exact (001) silicon substrates without the nucleation of threading dislocations and very thin buffer layers have been achieved.[112] Pulsed laser oscillation has been demonstrated, although efforts are needed to shift the lasing wavelength to the telecom range.[113,114] Also, GaSb can be grown on silicon in a wafer scale using a special mechanism in which most of the defects being formed remain confined to the interface. Room temperature lasing has been demonstrated.[115] From the prospective of integration, the relatively thick buffer layer (~ 2 μm) required for all the methods discussed above isolates the lasers from the silicon substrate however and it seems very challenging to couple light into the silicon waveguide underneath. Therefore, most demonstrations thus far relate to stand-alone lasers. A monolithic approach that allows intimate integration of III-Vs on silicon is highly demanded. In the following section, therefore, a selective growth technique is introduced that allows realizing almost buffer-free growth of high-quality InP and GaAs on exact (001) silicon substrates.

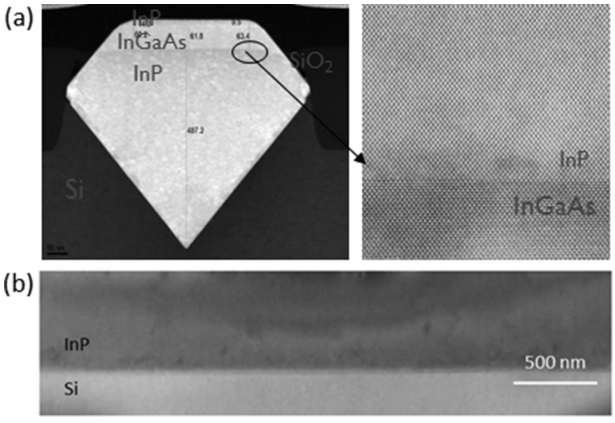

Figure 24. (a) STEM cross-section image and a zoom-in of the heterostructure of a InGaAs/InP/Si waveguide. (b) TEM image of a lamella prepared parallel to the 500 nm-wide InP-on-Si waveguide axis. (Reproduced from[119])

4.2. Buffer-Less Growth of III-V on (001) Silicon Substrates

The proposed process flow is summarized in **Figure 23**. Starting from a standard 300 mm (001) silicon substrate, using a shallow isolation trench (STI) process, an array of silicon ridges with widths varying from 10 nm to 500 nm are defined and planarized by a layer of SiO_2. Then, anisotropic etching of the silicon ridges is carried out using e.g. a Tetramethylammonium hydroxide (TMAH) solution (5% @ 80 °C). The two exposed <111> planes form a V-groove, which is important to avoid the formation of anti-phase domains during the subsequent III-V growth process.[116] The latter is carried out in a metal-organic vapor phase epitaxy (MOVPE) chamber. The deep STI sidewalls ensure defects are trapped in the trench. Threading dislocations generated during growth tend to glide along <111> planes, and will hit an oxide wall if the trench aspect ratio is sufficiently high. Also, planar defects on <111> planes can be easily trapped. Only the planar defects gliding in planes along to the trench are not trapped. Therefore, optimization of the low temperature nucleation process carried out at the start of the growth is critical. The temperature is then ramped up for growing high quality InP or GaAs in the trench. More details on the epitaxial growth can be found elsewhere.[116–118]

The shape of the material growing out of the trench is strongly dependent on the type of III-V semiconductor considered. In the case of InP/Si growth, stable triangle-shaped structures are formed, which are hard to control in terms of exact shape and dimensions. Therefore, a chemical mechanical polishing (CMP) process was developed to remove the overgrown InP, leaving a flat and clean InP surface. On top of that, a thin layer of InGaAs and a subsequent InP passivation layer were grown, forming a vertical heterostructure. A high angle annular dark field (HAADF) scanning transmission electron microscopy (STEM) image of a InP/InGaAs/InP/Si waveguide is shown in **Figure 24**a. The typical cross-sectional dimensions of the waveguide are about 500 nm by 500 nm. It shows that high-quality InP can be grown on silicon without buffer and most of the defects are

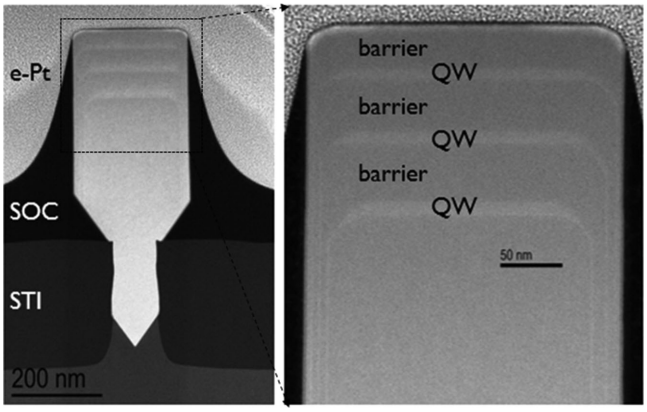

Figure 25. HAADF-STEM pictures of a GaAs waveguide with three InGaAs QWs. Left: Low-resolution cross-section image of the full waveguide. Right: A zoom-in of the multi-QW structure. Spin-on-carbon (SOC) and electron beam deposited platinum (e-Pt) were used as a capping layer. (Reproduced from[120])

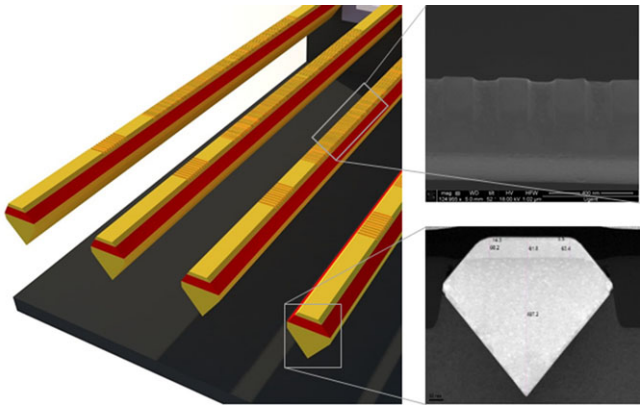

Figure 26. Schematic plot of the InGaAs/InP/Si laser array. Insert (upper): tilted SEM image of the DFB grating defined on the InGaAs/InP/Si waveguides. Insert (down): cross-section of the waveguide. (Reproduced from[119])

confined in a very thin defective layer (~30 nm) at the InP/Si interface.[121] The zoom-in image of the InGaAs/InP interface shows a very abrupt transition from the InP to the InGaAs layer, without evidence of misfits or threading dislocations. To estimate the defect density, a TEM image of a lamella prepared along the longitudinal direction of the InP/Si waveguide is shown in Figure 24b. No thresholding dislocations can be found, although planar defects such as stacking faults and twins occur occasionally, approximately at a rate of 0.2/μm.

When growing GaAs and related materials however, the growth recipe for GaAs is optimized such that the overgrown GaAs on top of the SiO_2 mask has a box shape, with a considerable growth in the lateral direction.[118] The shape of the box is determined by the relative growth rate of the top (001) surface and the (110) side walls. Facets along (111) are formed at the bottom of the box. The lateral width of the box can be in the order of a micrometer, which is comparable to the typical width of a "classical" III-V laser. The epitaxial growth can then be continued to grow the desired active layers, a stack of quantum wells (MQWs) at the top facets of the overgrown GaAs waveguide. **Figure 25** shows the HAADF-STEM pictures of a GaAs waveguide with three InGaAs QWs. The InGaAs QWs are clearly noticeable. Energy-dispersive X-ray spectroscopy (EDS) measurements determined an In content of 19%. Photoluminescence measurements (not shown here) show the material quality is excellent.[120]

4.3. O-Band Laser Array Monolithically Integrated on Silicon

Using the integration approach discussed above, DFB lasers have been previously demonstrated under pulsed optical pumping,[121] although their emission wavelength is ±920 nm, which is not compatible with silicon as a waveguide material. In this section, we present our recent demonstration of an O-band DFB laser.

The waveguide cross-section is shown in **Figure 26**, and the Indium content of the InGaAs layer was determined to be 35% by EDS measurement. Electron-beam lithography and a dry etching process are employed to define first order gratings in the top InP layer of the waveguide. A tilted side view of a suspended waveguide (20 nm grating etching depth) can be found in Figure 26. A more detailed process flow description can be found elsewhere.[119]

The emission spectrum of a single device below and above threshold is presented in **Figure 27**a. The measurement was carried out at room temperature on a micro-photoluminescence (μ-PL) setup. The pump source is a Nd:YAG nanosecond pulsed laser (1064 nm wavelength). Below threshold, the broad PL spectrum is centered at 1460 nm with two peaks. Simple strain analysis indicates that suspending the waveguide (to avoid substrate leakage) partially release the lattice constant mismatch at the InP/InGaAs interface, and the two peaks of the spectrum are most likely from heavy hole (HH) and light hole (LH) transitions. When increasing the pumping intensity, a laser peak appears at 1354 nm, and a side mode suppression ratio over 25 dB is measured. The relatively wide FWHM of the peak (1.8 nm) is believed to originate from carrier density modulation during the pulsed pumping.[122,123] Figure 27b shows the light-in-light-out (L-L) curve of the laser measured at room temperature. The red curve is a rate equation fit to the measured data (blue dots). A threshold pump power of 7.8 mW is obtained. Lasing under continuous wave pumping condition was not obtained, mostly due to the strong self-heating in the air-surrounded waveguide. The InP/InGaAs/InP heterostructure confines the carriers generated during optical pumping in the active layer and the fraction of carriers that recombine non-radiatively at the sidewalls is minimized. The threshold pumping density of the laser is derived to be around 10 kW/cm^2, an order of magnitude lower than for the previous InP/Si laser. Figure 27c shows the optical spectra of a 10 DFB laser array while gradually increasing grating period. Good control over the lasing wavelength and the relatively uniform output power across the array prove that the discussed integration approach provides the scalability needed by future high-density silicon photonic integrated circuits.

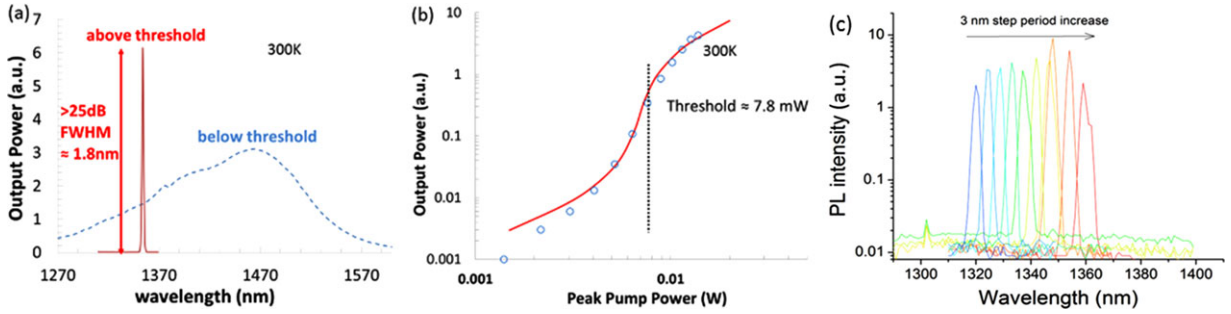

Figure 27. (a) Laser emission spectra below and above threshold. (b) Laser output power as a function of the input power (L-L curve). (c) The measured lasing spectra of a 10 DFB laser array, the grating period increases from 335 nm to 365 nm from left to right. (Reproduced from[119])

4.4. Discussion and Challenges

Monolithic integration of III-V lasers on silicon by epitaxial growth used to lag far behind other integration schemes. However, this field has gained strong momentum in the past few years. Most of the available techniques can be divided into two major categories: planar growth or selective growth. Given that with planar growth techniques layer stacks being very similar as those used in traditional III-V lasers can be grown, great progress has been made using this approach. Reliable, long term operation is now the focus,[109] and practical applications might come in the near future. However, from the integration point of view, most of the planar growth techniques still require thick buffer layers, which seems to prohibit close integration of III-V lasers with existing silicon photonic integrated circuits. Efficient schemes to couple the lasers to integrated waveguides are therefore highly demanded. More importantly, when photonic and electronic devices need to be co-integrated on the same chip, the use of such a non-selective growth technique may substantially complicate the process flow.

Selective growth techniques such as the V-groove-based approach discussed above on the other hand, show great promise for high-density co-integration of III-V photonic/electronic and Si photonic/electronic devices. Buffer-free growth facilitates the coupling of light between III-V and Si waveguides. Besides, the nature of the selective growth allows the processing of millions of III-V devices simultaneously without affecting any existing Si structures. However, this technology is still less mature. The next big leap is obviously the realization of electrically pumped lasers, which requires, amongst others, optimization of the doping process. Furthermore, because the material volume obtained by the selective growth is very limited, achieving efficient electrical injection without introducing a high free-carrier absorption loss or loss in the metal contacts is challenging. From this perspective, the GaAs-on-Si platform discussed above is a promising candidate, because a larger material volume can be grown. Ultimately, the reliability of devices grown using the buffer-less technique should be verified. It is not yet investigated whether the thin defective layer will expand during aging. Quantum dot-based active layers can again be a promising solution in this case, as it has been shown to be less sensitive to dislocations, as discussed above.

Last but not least, it is still an open debate whether monolithically integrated lasers can be compatible with CMOS-technology or not. Advanced CMOS transistors are rapidly becoming more and more diverse both in terms of material used and integration strategies (see ITRS roadmap, www.itrs.net). The monolithic laser presented above was partly processed (InP epitaxy, CMP) in a CMOS-pilot line operating under almost the same contamination conditions as those used in CMOS-foundries. In the same foundry, there have been various demonstrations of III-V based high-mobility electronic devices (InGaAs gate-all-around nanowire devices, InGaAs/InP quantum well finfet devices), which indicate that III-V electronic and photonic devices can be incorporated in a next generation CMOS fab. Regarding the concern of thermal budget compatibility, we envision that the photonic circuit, or the laser source only, can be processed at the very front-end stage, potentially right after the high temperature processing of certain electronic elements. In such circumstances, the low thermal budget of the following steps, such as metal contacts, will not be a constraint. A similar optimization was carried out when introducing Ge-detectors in a standard CMOS-flow, as was e.g. demonstrated industry.[124,125] Compared to some ongoing research activities such as silicon optical interposers, which decouple the processing of electronic and photonic chips for better thermal budget management, the monolithic integration approach is still an essential key technology that will enable future high volume and cost-sensitive applications.

5. Colloidal QD-based Light Emitters

5.1. Introduction

Colloidal quantum dots (QDs) are inorganic nanometer-sized semiconductor materials dispersed in solutions that are mostly prepared by wet-chemical synthesis. Due to their size-dependent quantum confinement effects, they have rich optical and electrical properties that can be engineered. In recent years, lots of efforts have been made to improve QD luminescence, which gives QDs great potential for the use in PICs to develop on-chip light sources such as lasers and single-photon emitters.[126] Various types of QDs have been shown to exhibit optical gain at wavelengths that can be readily adjusted from the near-infrared to visible wavelengths by selecting the proper material and size of the quantum dots.[127–129] Laser devices exploiting QD gain material were demonstrated over the last few years.[130–135] However, to bring their benefits also to photonic chips, an effective

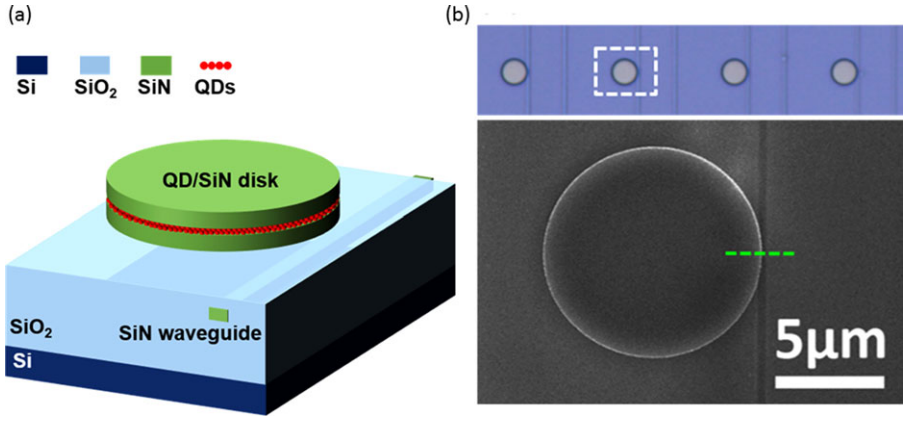

Figure 28. (a) Schematics of the device design. (b) Images of the fabricated devices. Top panel: microscope image of an array of devices on the chip. Bottom: top view SEM image of a selected device. (Reproduced from[138])

methodology to bring solution-processed QDs in a top-down PICs manufacturing process is needed. Therefore a technique for integrating QDs with silicon nitride (SiN) waveguide circuits has been developed recently.[136,137] The QDs do not degrade during this process whereby they are embedded into passive SiN waveguides. More importantly, by exploiting the wide-band transparency of SiN photonics and the broad spectral tunability of the QD emission, active PICs ranging from the visible to the near-infrared wavelengths can be envisaged.

5.2. Integrated Visible Light Colloidal QD Laser

Based on the hybrid QD/SiN integration platform, a first optically pumped on-chip QD/SiN microdisk laser has been demonstrated.[138,139] The microdisk comprises a SiN/QD/SiN sandwich that supports high Q whispering gallery modes (WGMs). The central CdSe/CdS core/shell QD layer is designed to achieve maximal overlap with cavity modes, providing optical gain around 630 nm wavelength. The active disk is vertically coupled to a passive SiN access waveguide for light coupling, as shown in **Figure 28**a. Figure 28b shows optical and scanning electron microscope (SEM) images of fabricated devices, revealing the achievement of a well-defined on-chip QD/SiN device.

The laser characterization was done on a μ-PL setup using a 400 nm pulsed laser with few picoseconds duration. **Figure 29a** shows the PL spectra of a 7 μm-diameter disk under different pump fluences. Below threshold (P_{th}), the spectrum exhibits typical WGM modes in the disk within the envelope of the broadband spontaneous emission of the QDs. When increasing the pump fluence to 1.16·P_{th}, a WGM mode at the center of the emission wavelength band starts lasing accompanied by a reduction in the line width. Further increasing the pump intensity to 1.80 P_{th} results in higher overall output and a second lasing mode. Figure 29b presents the total output intensity versus the pump fluence, clearly showing the lasing threshold of 27 μJ•cm^{-2}. Additionally, the log-scale L-L results for two lasing modes presented in the inset can be well fitted by a static rate equation model. The time-resolved PL further reveals a reduced lifetime from the spontaneous (1-2 ns) to the stimulated emission regime (3-6 ps). The characterization of temporal coherence of the laser beam indicates a distinct enhancement of coherence time above threshold. These results constitute a clear demonstration of ultra-compact on-chip QD/SiN microdisk lasers with a low threshold. The threshold of the laser device could be lowered even more by using different cavities or optimizing the QDs for higher optical gain. Some of our recent results have shown that by using a traditional distributed feedback (DFB) structure with the same hybrid QD/SiN integration platform, the laser can operate with nano-second pulsed laser pumping (7 ns pulse width), which is to the best of our knowledge a first for an integrated QD laser.[140] The lasing threshold power density is around 50kW/cm^2, which can be achieved by a focused CW laser. We are still investigating the possibility to realize a CW pumped QD laser, which would be a significant step towards practical applications. However, it is fundamentally challenging to do so due to the large area of defective surface covered by organic ligands. Furthermore, extending the laser wavelength from the visible to infrared wavelengths is another goal for the QD/SiN integration platform and this could be explored by taking advantage of the broad spectral tunability of the QD emission. This will open new avenues for optical communication and lab-on-a-chip sensing technologies.

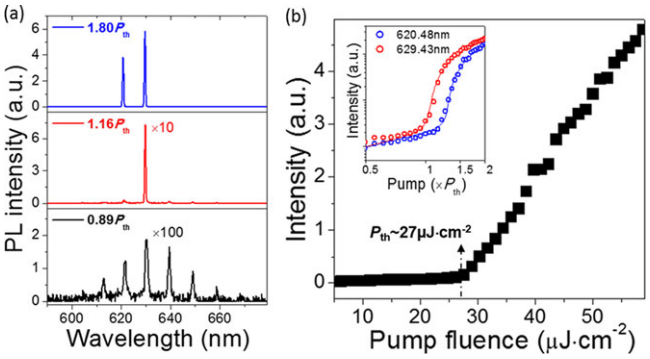

Figure 29. (a) The evolution of the PL spectrum of a 7 μm diameter disk with increasing pump fluence. (b) Measured Light(in)-Light(out) curve, showing a threshold of 27 μJ·cm-2. Inset: Log-scale L-L curves for two lasing modes. Symbols are measured data and solid lines are obtained by a rate equation fit. (Reproduced from[138])

Table 1. Comparison between different heterogeneous integration strategies on silicon

	Integration density	CMOS compatibility	Cost	Overall maturity
Heterogeneous bonding	Medium	Potentially back-end compatible	Medium	Mature
Transfer printing	High	Potentially back-end compatible	Low	R&D
Epitaxial growth	Very High	Potentially front-end compatible	Potentially very low	R&D
Colloidal QDs	High	Potentially back-end compatible	Potentially very low	Early R&D

Another research track aims at non-classical applications of QD-emitters. At the single dot level, QDs might be perfect candidates for realizing single photon sources.[141] Integrated in SiN waveguides the latter then could form the basis for fully integrated quantum optics experiments. We have already demonstrated that our "flash" single CdSe/CdS core/shell QD show photon anti-bunching when deposited on a glass substrate.[142] Furthermore, work of Bisschop et al[142] demonstrates that high coupling efficiency and polarization contrast can be attained in the simple silicon nitride waveguides. To realize a fully integrated single photon source on silicon photonic integrated circuits, accurately positioning the QDs is of paramount importance. Work by Xie et al. has shown a versatile and straightforward technique of positioning a single QD on a chip[143] by using lithography and lift-off processes. The technique can register a single QD in a desired location with a yield of up to 40% and thus provides an efficient tool for the development of on-chip devices based on a single QD.

6. Discussion and Conclusions

In this paper, recent progress in silicon-integrated novel light sources has been reviewed. Four integration approaches have been discussed. A comparison of various aspects of these technologies can be found in Table 1.

As one may expect, the heterogeneous bonding solution exhibits the highest maturity after years of extensive R&D. The discussed high-speed directly modulated InP/Si laser has a high bandwidth allowing 56 Gb/s operation, which is very promising for traditional datacom applications such as optical interconnects within hyper-scale datacenters. On the other hand, new laser configurations and functionalities are being explored for applications other than communications. By combining the advantages of III-V and Si material platforms, the recently demonstrated ultra-dense comb laser holds high promise for spectroscopy and microwave photonic applications, especially when combined with III-V-on-silicon waveguides for spectral broadening. The use of new III-V materials allows the extension of the laser wavelength range for various sensing applications. The recent announcement of the heterogeneous integration of III-V lasers in an optical transceiver product is an encouraging step for the further commercial deployment of such devices.[144] As discussed earlier, the heterogeneous bonding approach is very versatile in that it can be used to implement on-chip light sources for various applications as long as a critically flat interface can be prepared for bonding. Inheriting most of the properties of die-to-wafer bonding (see Table 1), transfer printing takes a step forward in the direction of large-scale integration. The automated alignment process, together with well-designed stamps, enable fast transfer of a large number of coupons to pre-patterned photonic chips. While transfer printing is already successfully being used in the photovoltaics industry and its application in display technology is emerging, the exploration of its application in photonic integrated circuits has just begun. The proof-of-concept demonstrations of wideband-emission LEDs and high-speed photodetectors show its great potential. Monolithic integration by epitaxial growth of III-Vs on silicon remains the ultimate solution for very high integration density applications such as on-chip optical interconnects. While planar growth has achieved comparable laser performance as its pure III-V counterparts, the introduced localized V-groove growth technique allows one to co-integrate III-V and Si photonic components as well as electronic devices while avoiding thick buffer layers and non-standard wafers. This technique, however, still requires extensive R&D to address challenges such as electrical pumping and reliability. The recent demonstration of an O-band monolithic laser array is an encouraging step towards a practically useful on-chip laser. Compared to the other approaches, using colloidal QDs as gain material for on-chip light sources is a relatively new research field. The low material and process cost and the capability of varying the emission wavelength from the visible to the near-IR – of interest for sensing applications - are the two major driving forces for the investments in this research topic. Limited by the intrinsic material properties, considerable fundamental work is still required to achieve lasing beyond the visible wavelength range. Electrical injection is also fundamentally difficult, however, recent progress in electrical pumped LEDs shows it is indeed feasible.[145] It is worth mentioning that thanks to the use of low-dimensional materials it is possible to realize a silicon-integrated single photon source by accurately positioning single quantum dots on pre-patterned photonic chips.

In summary, tremendous progress has been made in the past years, addressing the high demand for light sources integrated on silicon. The further evolution of the integration approaches discussed above may soon lead to diverse solutions that fit various application scenarios. One may conclude that the toolkit for silicon photonics, including integrated light sources, is now close to being complete.

Acknowledgements

This work is supported by the European Research Council (award numbers: 693447, 645314, 688519, 267853, 259076), the European Space Agency (ESA Artes 5.1 EPFC), the IAP P7/35 Photonics@BE project, and IMEC's industry-affiliation program on optical I/O.

Conflict of Interest

The authors have declared no conflict of interest.

Keywords

on-chip light sources, optical interconnections, silicon photonics, heterogeneous integration, transfer printing, III-V semiconductors, quantum dots

Received: March 16, 2017
Revised: June 1, 2017
Published online: July 6, 2017

[1] D. Liang and J. E. Bowers, *Nature Photonics* **4** (8), 511–517 (2010).
[2] K. Ohashi, K. Nishi, T. Shimizu, and M. Nakada, *Proceedings of the IEEE* **97** (7), 1186–1198 (2009).
[3] L. D. Negro, L. Pavesi, G. Pucker, G. Franzò, and F. Priolo, *Nature* **408** (6811), 440–444 (2000).
[4] O. Jambois, F. Gourbilleau, A. J. Kenyon, J. Montserrat, R. Rizk, and B. Garrido, *Opt. Express* **18** (3), 2230 (2010).
[5] S. Wirths, R. Geiger, N. von den Driesch, G. Mussler, T. Stoica, S. Mantl, Z. Ikonic, M. Luysberg, S. Chiussi, J. M. Hartmann, H. Sigg, J. Faist, D. Buca, and D. Grützmacher, *Nature Photonics* **9** (2), 88–92 (2015).
[6] R. E. Camacho-Aguilera, Y. Cai, N. Patel, J. T. Bessette, M. Romagnoli, L. C. Kimerling, and J. Michel, *Opt. Express* **20** (10), 11316–11320 (2012).
[7] L. Liu, R. Kumar, K. Huybrechts, T. Spuesens, G. Roelkens, E. J. Geluk, T. D. Vries, P. Regreny, D. V. Thourhout, and R. Baets, *Nature Photonics* **4**, 182–187 (2010).
[8] A. W. Fang, H. Park, O. Cohen, R. Jones, M. J. Paniccia, and J. E. Bowers, *Opt. Express* **14** (20), 9203 (2006).
[9] Z. Zhou, B. Yin, and J. Michel, *Light Science & Applications* **4** (11), e358 (2015).
[10] A. Z. Subramanian, E. Ryckeboer, A. Dhakal, F. Peyskens, A. Malik, B. Kuyken, H. Zhao, S. Pathak, A. Ruocco, A. De Groote, P. Wuytens, D. Martens, F. Leo, W. Xie, U. D. Dave, M. Muneeb, P. Van Dorpe, J. Van Campenhout, W. Bogaerts, P. Bienstman, N. Le Thomas, D. Van Thourhout, Z. Hens, G. Roelkens, and R. Baets, *Photonics Research* **3** (5), B47–B59 (2015).
[11] B. Bernhardt, A. Ozawa, P. Jacquet, M. Jacquey, Y. Kobayashi, T. Udem, R. Holzwarth, G. Guelachvili, T. W. Hansch, and N. Picque, *Nat Photon* **4** (1), 55–57 (2010).
[12] M. A. Foster, R. Salem, D. F. Geraghty, A. C. Turnerfoster, M. Lipson, and A. L. Gaeta, *Nature* **456** (7218), 81–84 (2008).
[13] J. W. Silverstone, D. Bonneau, J. L. O'Brien, and M. G. Thompson, *IEEE Journal of Selected Topics in Quantum Electronics* **22** (6), 390–402 (2016).
[14] H. W. Chen, A. W. Fang, J. D. Peters, and Z. Wang, *IEEE Transactions on Microwave Theory & Techniques* **58** (11), 3213–3219 (2010).
[15] J. Sun, E. Timurdogan, A. Yaacobi, E. S. Hosseini, and M. R. Watts, *Nature* **493** (7431), 195–199 (2013).
[16] M. Hermans, M. Burm, T. V. Vaerenbergh, J. Dambre, and P. Bienstman, *Nature Communications* **6** (s 1–3), 6729 (2015).
[17] C. Gunn, *IEEE Micro* **26** (2), 58–66 (2006).
[18] A. Abbasi, S. Keyvaninia, J. Verbist, X. Yin, J. Bauwelinck, F. Lelarge, G. H. Duan, G. Roelkens, and G. Morthier, *Journal of Lightwave Technology* **35** (6), 1235–1240 (2017).
[19] C. J. Van, R. P. Rojo, P. Regreny, C. Seassal, T. D. Van, S. Verstuyft, C. L. Di, J. M. Fedeli, C. Lagahe, and R. Baets, *Opt. Express* **15** (11), 6744 (2007).
[20] D. Liang, M. Fiorentino, T. Okumura, H. H. Chang, D. T. Spencer, Y. H. Kuo, A. W. Fang, D. Dai, R. G. Beausoleil, and J. E. Bowers, *Opt. Express* **17** (22), 20355 (2009).
[21] S. Keyvaninia, G. Roelkens, D. Van Thourhout, C. Jany, M. Lamponi, A. Le Liepvre, F. Lelarge, D. Make, G.-H. Duan, D. Bordel, and J.-M. Fedeli, *Opt. Express* **21** (3), 3784–3792 (2013).
[22] G. Kurczveil, M. J. R. Heck, J. D. Peters, and J. M. Garcia, *IEEE Journal of Selected Topics in Quantum Electronics* **17** (6), 1521–1527 (2011).
[23] G. Roelkens, L. Liu, D. Liang, R. Jones, A. Fang, B. Koch, and J. Bowers, *Laser & Photonics Review* **4** (4), 751–779 (2010).
[24] T. Komljenovic, S. Srinivasan, E. Norberg, M. Davenport, G. Fish, and J. E. Bowers, *IEEE Journal of Selected Topics in Quantum Electronics* **21** (6), 214–222 (2015).
[25] S. Srinivasan, M. Davenport, M. J. R. Heck, J. Hutchinson, E. Norberg, G. Fish, and J. Bowers, *Frontiers of Optoelectronics* **7** (3), 265–276 (2014).
[26] C. T. Santis, S. T. Steger, Y. Vilenchik, A. Vasilyev, and A. Yariv, *Proceedings of the National Academy of Sciences* **111** (8), 2879–2884 (2014).
[27] J. C. Hulme, J. K. Doylend, and J. E. Bowers, *Opt. Express* **21** (17), 19718–19722 (2013).
[28] G. H. Duan, C. Jany, A. L. Liepvre, A. Accard, M. Lamponi, D. Make, P. Kaspar, G. Levaufre, N. Girard, F. Lelarge, J. M. Fedeli, A. Descos, B. B. Bakir, S. Messaoudene, D. Bordel, S. Menezo, G. d. Valicourt, S. Keyvaninia, G. Roelkens, D. V. Thourhout, D. J. Thomson, F. Y. Gardes, and G. T. Reed, *IEEE Journal of Selected Topics in Quantum Electronics* **20** (4), 158–170 (2014).
[29] T. Creazzo, E. Marchena, S. B. Krasulick, P. K. L. Yu, D. Van Orden, J. Y. Spann, C. C. Blivin, L. He, H. Cai, J. M. Dallesasse, R. J. Stone, and A. Mizrahi, *Opt. Express* **21** (23), 28048–28053 (2013).
[30] G. Kurczveil, M. J. R. Heck, J. D. Peters, J. M. Garcia, D. Spencer, and J. E. Bowers, *IEEE Journal of Selected Topics in Quantum Electronics* **17** (6), 1521–1527 (2011).
[31] X. Zheng, S. Lin, Y. Luo, J. Yao, G. Li, S. S. Djordjevic, J. H. Lee, H. D. Thacker, I. Shubin, K. Raj, J. E. Cunningham, and A. V. Krishnamoorthy, *Journal of Lightwave Technology* **31** (24), 4142–4154 (2013).
[32] G. D. Valicourt, G. Levaufre, Y. Pointurier, A. L. Liepvre, J. C. Antona, C. Jany, A. Accard, F. Lelarge, D. Make, and G. H. Duan, *Journal of Lightwave Technology* **33** (8), 1608–1616 (2015).
[33] C. Zhang, S. Srinivasan, Y. Tang, M. J. R. Heck, M. L. Davenport, and J. E. Bowers, *Opt. Express* **22** (9), 10202–10209 (2014).
[34] K. Nakahara, Y. Wakayama, T. Kitatani, T. Taniguchi, T. Fukamachi, Y. Sakuma, and S. Tanaka, *IEEE Photonics Technology Letters* **27** (5), 534–536 (2015).
[35] D. M. Kuchta, T. N. Huynh, F. E. Doany, L. Schares, C. W. Baks, C. Neumeyr, A. Daly, B. Kögel, J. Rosskopf, and M. Ortsiefer, *Journal of Lightwave Technology* **34** (14), 3275–3282 (2016).
[36] G. Morthier, R. Schatz, and O. Kjebon, *IEEE Journal of Quantum Electronics* **36** (12), 1468–1475 (2000).
[37] Y. Urino, T. Usuki, J. Fujikata, M. Ishizaka, K. Yamada, T. Horikawa, T. Nakamura, and Y. Arakawa, *Photonics Research* **2** (3), A1–A7 (2014).
[38] C. Zhang, S. Zhang, J. D. Peters, and J. E. Bowers, *Optica* **3** (7), 785–786 (2016).
[39] G. Crosnier, D. Sanchez, S. Bouchoule, P. Monnier, G. Beaudoin, I. Sagnes, R. Raj, and F. Raineri, *Nat Photon* **11** (5), 297–300 (2017).
[40] O. Painter, R. K. Lee, A. Scherer, A. Yariv, J. D. O'Brien, P. D. Dapkus, and I. Kim, *Science* **284** (5421), 1819–1821 (1999).
[41] B. Ellis, M. A. Mayer, G. Shambat, T. Sarmiento, J. Harris, E. E. Haller, and J. Vuckovic, *Nat Photon* **5** (5), 297–300 (2011).
[42] S. Keyvaninia, S. Verstuyft, L. Van Landschoot, F. Lelarge, G. H. Duan, S. Messaoudene, J. M. Fedeli, T. De Vries, B. Smalbrugge, E. J. Geluk, J. Bolk, M. Smit, G. Morthier, D. Van Thourhout, and G. Roelkens, *Opt. Lett.* **38** (24), 5434–5437 (2013).
[43] F. This result was obtained through collaboration with III-V labs.

[44] A. Abbasi, B. Moeneclaey, J. Verbist, X. Yin, J. Bauwelinck, G. H. Duan, G. Roelkens, and G. Morthier, *IEEE Journal of Selected Topics in Quantum Electronics* **PP** (99), 1–1 (2017).
[45] A. Abbasi, B. Moeneclaey, J. Verbist, X. Yin, J. Bauwelinck, G. Roelkens, and G. Morthier, in *Optical Fiber Communication Conference (OFC)*, edited by OSA (Los Angeles, United States, 2017).
[46] P. J. Delfyett, D. H. Hartman, and S. Z. Ahmad, *Journal of Lightwave Technology* **9** (12), 1646–1649 (1991).
[47] J. Mandon, G. Guelachvili, and N. Picque, *Nat Photon* **3** (2), 99–102 (2009).
[48] E. Hamidi, D. E. Leaird, and A. M. Weiner, *IEEE Transactions on Microwave Theory & Techniques* **58** (11), 3269–3278 (2010).
[49] B. R. Washburn, S. A. Diddams, N. R. Newbury, J. W. Nicholson, M. F. Yan, and C. G. Jørgensen, *Opt. Lett.* **29** (3), 250–252 (2004).
[50] T. Ideguchi, S. Holzner, B. Bernhardt, G. Guelachvili, N. Picque, and T. W. Hansch, *Nature* **502** (7471), 355–358 (2013).
[51] G. Millot, S. Pitois, M. Yan, T. Hovhannisyan, A. Bendahmane, T. W. Hänsch, and N. Picqué, *Nat Photon* **10** (1), 27–30 (2016).
[52] J. S. Levy, A. Gondarenko, M. A. Foster, A. C. Turner-Foster, A. L. Gaeta, and M. Lipson, *Nat Photon* **4** (1), 37–40 (2010).
[53] K. Mori and K. Sato, *IEEE Photonics Technology Letters* **17** (2), 480–482 (2005).
[54] S. Cheung, J. H. Baek, R. P. Scott, N. K. Fontaine, F. M. Soares, X. Zhou, D. M. Baney, and S. J. B. Yoo, *IEEE Photonics Technology Letters* **22** (24), 1793–1795 (2010).
[55] S. Latkowski, V. Moskalenko, S. Tahvili, L. Augustin, M. Smit, K. Williams, and E. Bente, *Opt. Lett.* **40** (1), 77–80 (2015).
[56] Y. Li, M. Breivik, C. Y. Feng, B. O. Fimland, and L. F. Lester, *IEEE Photonics Technology Letters* **23** (14), 1019–1021 (2011).
[57] B. R. Koch, A. W. Fang, O. Cohen, and J. E. Bowers, *Opt. Express* **15** (18), 11225–11233 (2007).
[58] Z. Wang, K. Van Gasse, V. Moskalenko, S. Latkowski, E. Bente, B. Kuyken, and G. Roelkens, *Light Sci Appl.* **6**, e16260 (2017).
[59] T. N. This result was obtained through collaboration with Eindhoven University of Technology.
[60] S. Keyvaninia, S. Uvin, M. Tassaert, Z. Wang, X. Fu, S. Latkowski, J. Marien, L. Thomassen, F. Lelarge, and G. Duan, *Opt. Lett.* **40** (13), 3057–3060 (2015).
[61] J. Javaloyes and S. Balle, *Opt. Lett.* **36** (22), 4407–4409 (2011).
[62] B. W. Tilma, M. Mangold, C. A. Zaugg, S. M. Link, D. Waldburger, A. Klenner, A. S. Mayer, E. Gini, M. Golling, and U. Keller, *Light Sci Appl* **4**, e310 (2015).
[63] A. Apolonski, A. Poppe, G. Tempea, C. Spielmann, T. Udem, R. Holzwarth, T. W. Hänsch, and F. Krausz, *Physical Review Letters* **85** (4), 740–743 (2000).
[64] S. Uvin, S. Keyvaninia, F. Lelarge, G.-H. Duan, B. Kuyken, and G. Roelkens, *Opt. Express* **24** (5), 5277–5286 (2016).
[65] J. S. Levy, A. Gondarenko, M. A. Foster, A. C. Turnerfoster, A. L. Gaeta, and M. Lipson, *Nature Photonics* **4** (1), 37–40 (2009).
[66] L. Razzari, D. Duchesne, M. Ferrera, R. Morandotti, S. Chu, B. E. Little, and D. J. Moss, *Nature Photonics* **4** (1), 41–45 (2009).
[67] A. G. Griffith, *Nature Communications* **6**, 1–2 (2015).
[68] H. Jung, R. Stoll, X. Guo, D. Fischer, and H. X. Tang, *Optica* **1** (6), 396–399 (2014).
[69] M. Pu, L. Ottaviano, E. Semenova, and K. Yvind, *Optica* **3** (8), 823–826 (2016).
[70] U. D. Dave, C. Ciret, S. P. Gorza, S. Combrie, R. A. De, F. Raineri, G. Roelkens, and B. Kuyken, *Opt. Lett.* **40** (15), 3584–3587 (2015).
[71] U. D. Dave, B. Kuyken, F. Leo, S. P. Gorza, S. Combrie, R. A. De, F. Raineri, and G. Roelkens, *Opt. Express* **23** (4), 4650 (2015).
[72] B. This result was obtained through collaboration with Université Libre de Bruxelles.
[73] S. Coen, H. G. Randle, T. Sylvestre, and M. Erkintalo, *Opt. Lett.* **38** (1), 37–39 (2012).
[74] J. Pfeifle, V. Brasch, M. Lauermann, Y. Yu, D. Wegner, T. Herr, K. Hartinger, P. Schindler, J. Li, and D. Hillerkuss, *Nature Photonics* **8** (5), 375–380 (2014).
[75] V. Brasch, E. Lucas, J. D. Jost, M. Geiselmann, and T. J. Kippenberg, *Light Sci Appl.* **6**, e16202 (2017).
[76] A. Spott, M. Davenport, J. Peters, J. Bovington, M. J. Heck, E. J. Stanton, I. Vurgaftman, J. Meyer, and J. Bowers, *Opt. Lett.* **40** (7), 1480–1483 (2015).
[77] R. Wang, S. Sprengel, G. Boehm, M. Muneeb, R. Baets, M. C. Amann, and G. Roelkens, *Opt. Express* **24** (18), 21081–21089 (2016).
[78] R. Wang, S. Sprengel, A. Malik, A. Vasiliev, G. Boehm, R. Baets, M. C. Amann, and G. Roelkens, *Applied Physics Letters* **109** (22), 221111 (2016).
[79] G. This result was obtained through collaboration with the Technical University of Munich.
[80] S. Sprengel, G. K. Veerabathran, A. Andrejew, A. Köninger, G. Boehm, C. Grasse, and M. C. Amann, *Proceedings of SPIE - The International Society for Optical Engineering* **9382**, 93820U-93820U-93826 (2015).
[81] E. Haglund, P. Westbergh, J. S. Gustavsson, and E. P. Haglund, *Electronics Letters* **51** (14), 1096–1098 (2015).
[82] D. M. Kuchta, A. V. Rylyakov, F. E. Doany, C. L. Schow, J. E. Proesel, C. W. Baks, P. Westbergh, J. S. Gustavsson, and A. Larsson, *IEEE Photonics Technology Letters* **27** (6), 1–1 (2015).
[83] Y. Yang, G. Djogo, M. Haque, P. R. Herman, and J. K. S. Poon, *Opt. Express* **25** (5), 5758–5771 (2017).
[84] K. S. Kaur, A. Z. Subramanian, P. Cardile, R. Verplancke, J. Van Kerrebrouck, S. Spiga, R. Meyer, J. Bauwelinck, R. Baets, and G. Van Steenberge, *Opt. Express* **23** (22), 28264–28270 (2015).
[85] H. Lu, J. S. Lee, Y. Zhao, C. Scarcella, P. Cardile, A. Daly, M. Ortsiefer, L. Carroll, and P. O'Brien, *Opt. Express* **24** (15), 16258–16266 (2016).
[86] J. Ferrara, W. Yang, L. Zhu, P. Qiao, and C. J. Chang-Hasnain, *Opt. Express* **23** (3), 2512–2523 (2015).
[87] G. C. Park, W. Xue, A. Taghizadeh, E. Semenova, K. Yvind, J. Mørk, and I.-S. Chung, *Laser & Photonics Reviews* **9** (3), L11–L15 (2015).
[88] D. A. Louderback, G. W. Pickrell, H. C. Lin, M. A. Fish, J. J. Hindi, and P. S. Guilfoyle, *Electronics Letters* **40** (17), 1064–1065 (2004).
[89] E. P. Haglund, S. Kumari, P. Westbergh, J. S. Gustavsson, G. Roelkens, R. Baets, and A. Larsson, *Opt. Express* **23** (26), 33634–33640 (2015).
[90] E. P. Haglund, S. Kumari, P. Westbergh, and J. S. Gustavsson, *IEEE Photonics Technology Letters* **28** (8), 856–859 (2016).
[91] E. P. Haglund, S. Kumari, E. Haglund, J. S. Gustavsson, R. G. Baets, G. Roelkens, and A. Larsson, *IEEE Journal of Selected Topics in Quantum Electronics* **23** (6), 1–9 (2017).
[92] S. This result was obtained through collaboration with Chalmers University of Technology.
[93] E. Menard, K. J. Lee, D. Y. Khang, and R. G. Nuzzo, *Applied Physics Letters* **84** (26), 5398–5400 (2004).
[94] M. A. Meitl, Z. T. Zhu, V. Kumar, K. J. Lee, X. Feng, Y. Y. Huang, I. Adesida, R. G. Nuzzo, and J. A. Rogers, *Nature Material* **5** (1), 33–38 (2005).
[95] A. D. Groote, P. Cardile, A. Z. Subramanian, A. M. Fecioru, C. Bower, D. Delbeke, R. Baets, and G. Roelkens, *Opt. Express* **24** (13), 13754 (2016).
[96] J. Justice, C. Bower, M. Meitl, M. B. Mooney, M. A. Gubbins, and B. Corbett, *Nature Photonics* **6** (9), 612–616 (2012).
[97] H. Yang, D. Zhao, S. Chuwongin, J. H. Seo, W. Yang, Y. Shuai, J. Berggren, M. Hammar, Z. Ma, and W. Zhou, *Nature Photonics* **6** (6), 617–622 (2012).
[98] A. J. Trindade, B. Guilhabert, D. Massoubre, D. Zhu, N. Laurand, E. Gu, I. M. Watson, C. J. Humphreys, and M. D. Dawson, *Applied Physics Letters* **103** (25), 239_231 (2013).

[99] I. This result was obtained through collaboration with Tyndall National Institute and X-Celeprint.
[100] J. Zhang, Y. Li, S. Dhoore, G. Morthier, and G. Roelkens, *Opt. Express* **25** (6), 7092–7100 (2017).
[101] T. H. Kim, K. S. Cho, E. K. Lee, J. L. Sang, J. Chae, J. W. Kim, D. H. Kim, J. Y. Kwon, G. Amaratunga, and Y. L. Sang, *Nature Photonics* **5** (3), 176–182 (2011).
[102] S. Dhoore, S. Uvin, T. D. Van, G. Morthier, and G. Roelkens, *Opt. Express* **24** (12), 12976 (2016).
[103] T. Shimizu, N. Hatori, M. Kurihara, Y. Urino, T. Yamamoto, T. Nakamura, and Y. Arakawa, *Photonics* **2** (4), 1131 (2015).
[104] T. Frost, S. Jahangir, E. Stark, S. Deshpande, A. Hazari, C. Zhao, B. S. Ooi, and P. Bhattacharya, *Nano Letters* **14** (8), 4535–4541 (2014).
[105] Y. Wan, Q. Li, A. Y. Liu, A. C. Gossard, J. E. Bowers, E. L. Hu, and K. M. Lau, *Opt. Lett.* **41** (7), 1664 (2016).
[106] H. Sun, F. Ren, K. W. Ng, T.-T. D. Tran, K. Li, and C. J. Chang-Hasnain, *ACS Nano* **8** (7), 6833–6839 (2014).
[107] R. Chen, T.-T. D. Tran, K. W. Ng, W. S. Ko, L. C. Chuang, F. G. Sedgwick, and C. Chang-Hasnain, *Nat Photon* **5** (3), 170–175 (2011).
[108] A. Y. Liu, C. Zhang, J. Norman, A. Snyder, D. Lubyshev, J. M. Fastenau, A. W. K. Liu, A. C. Gossard, and J. E. Bowers, *Applied Physics Letters* **104** (4), 041104 (2014).
[109] S. Chen, W. Li, J. Wu, Q. Jiang, M. Tang, S. Shutts, S. N. Elliott, A. Sobiesierski, A. J. Seeds, I. Ross, P. M. Smowton, and H. Liu, *Nat Photon* **10** (5), 307–311 (2016).
[110] S. Mitsuru, M. Hidefumi, I. Yoshio, S. Yoshihisa, and T. Masami, *Japanese Journal of Applied Physics* **30** (12S), 3876 (1991).
[111] S. Chen, M. Liao, M. Tang, J. Wu, M. Martin, T. Baron, A. Seeds, and H. Liu, *Opt. Express* **25** (5), 4632–4639 (2017).
[112] K. Volz, A. Beyer, W. Witte, J. Ohlmann, I. Németh, B. Kunert, and W. Stolz, *Journal of Crystal Growth* **315** (1), 37–47 (2011).
[113] N. Hossain, S. J. Sweeney, S. Rogowsky, R. Ostendorf, J. Wagner, S. Liebich, M. Zimprich, K. Volz, B. Kunert, and W. Stolz, *Electronics Letters* **47** (16), 931–933 (2011).
[114] X. Huang, Y. Song, T. Masuda, and D. Jung, *Electronics Letters* **50** (17), 1226–1227 (2014).
[115] J. R. Reboul, L. Cerutti, J. B. Rodriguez, P. Grech, and E. Tournie, *Applied Physics Letters* **99** (12), 121113-121113-3 (2011).
[116] M. Paladugu, C. Merckling, R. Loo, O. Richard, H. Bender, J. Dekoster, W. Vandervorst, M. Caymax, and M. Heyns, *Crystal Growth & Design* **12** (10), 4696–4702 (2012).
[117] C. Merckling, N. Waldron, S. Jiang, W. Guo, N. Collaert, M. Caymax, E. Vancoille, K. Barla, A. Thean, M. Heyns, and W. Vandervorst, *Journal of Applied Physics* **115** (2), 023710 (2014).
[118] B. Kunert, W. Guo, Y. Mols, R. Langer, and K. Barla, *Ecs Transactions* **75** (8), 409–419 (2016).
[119] B. Tian, Z. Wang, M. Pantouvaki, P. Absil, J. Van Campenhout, C. Merckling, and D. Van Thourhout, *Nano Letters* **17** (1), 559–564 (2017).
[120] B. Kunert, W. Guo, Y. Mols, B. Tian, Z. Wang, Y. Shi, D. V. Thourhout, M. Pantouvaki, J. V. Campenhout, and R. Langer, *Applied Physics Letters* **109** (9), 091101 (2016).
[121] Z. Wang, B. Tian, M. Pantouvaki, W. Guo, P. Absil, J. V. Campenhout, C. Merckling, and D. V. Thourhout, *Nature Photonics* **9** (12) (2015).
[122] Z. Wang, B. Tian, M. Pantouvaki, W. Guo, P. Absil, J. Van Campenhout, C. Merckling, and D. Van Thourhout, *Nat Photon* **9** (12), 837–842 (2015).
[123] T. L. Koch, and J. E. Bowers, *Electronics Letters* **20** (25), 1038–1040 (1984).
[124] G. Masini, S. Sahni, G. Capellini, J. Witzens, and C. Gunn, *Advances in Optical Technologies* **2008**, 5 (2008).
[125] S. J. Koester, C. L. Schow, L. Schares, G. Dehlinger, J. D. Schaub, F. E. Doany, and R. A. John, *Journal of Lightwave Technology* **25** (1), 46–57 (2007).
[126] M. Cirillo, T. Aubert, R. Gomes, R. V. Deun, P. Emplit, A. Biermann, H. Lange, C. Thomsen, E. Brainis, and Z. Hens, *Chemistry of Materials* **26** (2), 1154–1160 (2013).
[127] V. I. Klimov, A. A. Mikhailovsky, S. Xu, A. Malko, J. A. Hollingsworth, C. A. Leatherdale, H. Eisler, and M. G. Bawendi, *Science* **290** (5490), 314–317 (2000).
[128] J. Q. Grim, S. Christodoulou, S. F. Di, R. Krahne, R. Cingolani, L. Manna, and I. Moreels, *Nature Nanotechnology* **9** (11), 891–895 (2014).
[129] C. She, I. Fedin, D. S. Dolzhnikov, P. D. Dahlberg, G. S. Engel, R. D. Schaller, and D. V. Talapin, *Acs Nano* **9** (10), 9475–9485 (2015).
[130] C. Grivas, C. Li, P. Andreakou, P. Wang, M. Ding, G. Brambilla, L. Manna, and P. Lagoudakis, *Nature Communications* **4** (4), 1161–1171 (2013).
[131] A. H. Ip, S. M. Thon, S. Hoogland, O. Voznyy, D. Zhitomirsky, R. Debnath, L. Levina, L. R. Rollny, G. H. Carey, and A. Fischer, *Nature Nanotechnology* **7** (9), 577–582 (2012).
[132] R. D. Schaller, M. A. Petruska, and V. I. Klimov, *Cheminform* **107** (50), 13765–13768 (2003).
[133] V. I. Klimov, S. A. Ivanov, J. Nanda, M. Achermann, I. Bezel, J. A. Mcguire, and A. Piryatinski, *Nature* **447** (7143), 441–446 (2007).
[134] H. Eisler, V. C. Sundar, M. G. Bawendi, M. Walsh, H. I. Smith, and V. Klimov, *Applied Physics Letters* **80** (80), 4614–4616 (2002).
[135] Y. Wang, V. D. Ta, Y. Gao, T. C. He, R. Chen, E. Mutlugun, H. V. Demir, and H. D. Sun, *Advanced Materials* **26** (18), 2954–2961 (2014).
[136] W. Xie, Y. Zhu, T. Aubert, S. Verstuyft, Z. Hens, and D. V. Thourhout, *Opt. Express* **23** (9), 12152–12160 (2015).
[137] W. Xie, Y. Zhu, T. Aubert, Z. Hens, E. Brainis, and T. D. Van, *Opt. Express* **24** (2), A114 (2016).
[138] W. Xie, T. Stöferle, G. Rainò, T. Aubert, S. Bisschop, Y. Zhu, R. F. Mahrt, P. Geiregat, E. Brainis, Z. Hens, and D. Van Thourhout, *Advanced Materials* **29** (16), 1604866-n/a (2017).
[139] T. r. w. o. t. c. w. IBM-Zurich.
[140] Y. Zhu, W. Xie, P. Geiregat, S. Bisschop, T. Aubert, E. Brainis, Z. hens, and D. Van Thourhout, presented at the Conference on Lasers and Electro-Optics, San Jose, California, 2017 (unpublished).
[141] X. Brokmann, G. Messin, P. Desbiolles, E. Giacobino, M. Dahan, and J. P. Hermier, *New Journal of Physics* **6** (5) (2004).
[142] S. Bisschop, A. Guille, T. D. Van, Z. Hens, and E. Brainis, *Opt. Express* **23** (11), 13713 (2015).
[143] W. Xie, R. Gomes, T. Aubert, S. Bisschop, Y. Zhu, Z. Hens, E. Brainis, and D. V. Thourhout, *Nano Letters* **15** (11), 7481–7487 (2015).
[144] http://www.intel.com/content/www/us/en/architecture-and-technology/silicon-photonics/silicon-photonics-overview.html.
[145] X. Dai, Z. Zhang, Y. Jin, Y. Niu, H. Cao, X. Liang, L. Chen, J. Wang, and X. Peng, *Nature* **515** (7525), 96 (2014).